Hindawi
Advances in High Energy Physics
Volume 2024, Article ID 9339959, 26 pages
https://doi.org/10.1155/2024/9339959

Research Article

Statistical Issues on the Neutrino Mass Hierarchy with $\Delta\chi^2$

F. Sawy [1] and L. Stanco [2]

[1] *American University in Cairo, Cairo, Egypt*
[2] *INFN, Sezione di Padova, 35131 Padova, Italy*

Correspondence should be addressed to F. Sawy; fatma.helal@aucegypt.edu

Received 10 October 2023; Revised 24 January 2024; Accepted 29 March 2024; Published 14 May 2024

Academic Editor: Subhash Singha

The neutrino mass hierarchy determination (ν MHD) is one of the main goals of the major current and future neutrino experiments. The statistical analysis usually proceeds from a standard method, a single-dimensional estimator $(1\text{D} - \Delta\chi^2)$ that shows some drawbacks and concerns, together with a debatable strategy. The drawbacks and considerations of the standard method will be explained through the following three main issues. The first issue corresponds to the limited power of the standard method. The $\Delta\chi^2$ estimator provides us with different results when different simulation procedures were used. Regarding the second issue, when $\chi^2_{\text{min (NH)}}$ and $\chi^2_{\text{min (IH)}}$ are drawn in a 2D map, their strong positive correlation manifests χ^2 as a bidimensional variable, instead of a single-dimensional estimator. The overlapping between the χ^2 distributions of the two hypotheses leads to an experiment sensitivity reduction. The third issue corresponds to the robustness of the standard method. When the JUNO sensitivity is obtained using different procedures, either with $\Delta\chi^2$ as one-dimensional or χ^2 as two-dimensional estimator, the experimental sensitivity varies with the different values of the atmospheric mass, the input parameter. We computed the oscillation of $|\overline{\Delta\chi^2}|$ with the input parameter values, $|\Delta m^2|_{\text{input}}$. The MH significance using the standard method, $\Delta\chi^2$, strongly depends on the values of the parameter $|\Delta m^2|_{\text{input}}$. Consequently, the experiment sensitivity depends on the precision of the atmospheric mass. This evaluation of the standard method confirms the drawbacks.

1. Introduction

Neutrino oscillation is a quantum mechanical phenomenon in which neutrino flavor changes spontaneously to another flavor. According to the standard 3 neutrino paradigm, neutrinos come with three flavors, ν_e, ν_μ, and ν_τ, and with three ν_1, ν_2, and ν_3 mass eigenstates [1]. Although neutrinos were introduced over 80 years ago, their properties remain to a large extent unknown [2]. Some of the 3ν–paradigm fundamental parameters are still missing until now like the absolute masses of neutrinos [3], the amount of the possible leptonic charge parity violation (CPV) [4], the Dirac or Majorana neutrino nature [5], and the neutrino mass ordering [6].

Currently, the determination of the neutrino mass ordering using reactor neutrino spectrum is pursued by several experiments and proposals. There are some challenges facing anyone that tries to solve this problem. First, its evaluation from reactor experiments is based on the tiny interference effect between the Δm^2_{31} and Δm^2_{23} oscillations [7]. Second, current analyses require several years of data taking and an extreme energy resolution to achieve anyhow less than 5σ. Third, the sensitivity may depend on the input values of the oscillation parameters used by the global fits on the oscillation analysis. In particular, the neutrino atmospheric mass may have different values for normal ordering (NH) or inverted one (IH). The answer to the third point depends on the used analysis method. It is mandatory to establish the robustness of all these analyses.

The Jiangmen Underground Neutrino Observatory (JUNO) experiment [8] has been proposed and approved for realization in the south of China, being the mass ordering (MO) evaluation one of its main goals. JUNO will allow to single out one of the missing fundamental information, the neutrino mass hierarchy, in an almost independent way of the other neutrino parameters. In particular, there will be no dependence on the phase of the leptonic CP violation, δ_{CP}, no strong dependence on three vs four neutrino pattern, no dependence on θ_{13}, and no dependence on matter effects [8]. The mass hierarchy study can be performed by looking at the vacuum oscillation pattern in medium baseline reactor antineutrino experiments [9]. The JUNO strategy is based on the observation that the contribution to the oscillation probability is represented by fast oscillating terms superimposed to a general oscillation pattern. Their relative size changes according to the two different possibilities, NH or IH, leading to a contribution of opposite sign in the two cases. Therefore, it is possible to discriminate between the two possible mass hierarchies by studying the interference between the two oscillation frequencies driven by Δm^2_{31} and Δm^2_{23} in the reactor antineutrino spectrum [10]. The discrimination power of the experiment is maximized when the Δm^2_{21} oscillation is maximal, and the baseline at JUNO has been chosen in such a way to realize this condition [11]. Since the difference of neutrino oscillation in vacuum for different mass hierarchies is very small, energy resolution is the crucial factor for the success of JUNO. The goal is that the energy resolution reaches $3\%/\sqrt{E}$ at 1 MeV to detect electron neutrino coming from reactor plants.

In the next section, the usual χ^2 method is recollected and evaluated. In the following sections, the three issues of the standard algorithm are explained. Section 3 includes the first issue, Section 4 explains the second issue, and the third issue is accounted for in Section 5. Further, results are described in Section 6. After that, conclusions are drawn in Section 7. Finally, in the appendix, a technical description of the implementation of the simulations is reported.

2. The Standard Method

For JUNO, χ^2 can be divided into three parts as indicated:

$$\chi^2 = \chi^2_{\text{para}} + \chi^2_{\text{sys}} + \chi^2_{\text{stat}}. \tag{1}$$

χ^2_{para} summarizes the prior knowledge on oscillation parameters. In JUNO, these parameters are $\sin^2 2\theta_{12}$, $\sin^2 2\theta_{13}$, δm^2_{sol} and Δm^2. Then, χ^2_{para} becomes

$$\chi^2_{\text{para}} = \left(\frac{\left(\sin^2 2\theta_{12}\right)^{\text{fit}} - \left(\sin^2 2\theta_{12}\right)^{\text{input}}}{\sigma_{\sin^2 2\theta_{12}}}\right)^2 + \left(\frac{\left(\sin^2 2\theta_{13}\right)^{\text{fit}} - \left(\sin^2 2\theta_{13}\right)^{\text{input}}}{\sigma_{\sin^2 2\theta_{13}}}\right)^2 + \left(\frac{\left(\left|\Delta m^2\right|\right)^{\text{fit}} - \left(\left|\Delta m^2\right|\right)^{\text{input}}}{\sigma_{\left|\Delta m^2\right|}}\right)^2 + \left(\frac{\left(\delta m^2_{\text{sol}}\right)^{\text{fit}} - \left(\delta m^2_{\text{sol}}\right)^{\text{input}}}{\sigma_{\delta m^2_{\text{sol}}}}\right)^2. \tag{2}$$

Table 1: The recent best-fit values for the oscillation parameters, as indicated in [12].

	Best-fit	3σ region
Sin^2_{12}	0.2970	0.2500-0.3540
Sin^2_{13}(NH)	0.02140	0.0185-0.0246
Sin^2_{13}(IH)	0.02180	0.0186-0.0248
δm^2_{sol}	7.37×10^{-5}	$6.93 \times 10^{-5} - 7.97 \times 10^{-5}$
Δm^2(NH)	2.500×10^{-3}	$2.37 \times 10^{-3} - 2.63 \times 10^{-3}$
Δm^2(IH)	2.460×10^{-3}	-2.60×10^{-3} to -2.33×10^{-3}

While the total normalization of reactor antineutrino flux is in principle degenerate with the inverted beta decay cross section, the fiducial volume, and the weight fraction of free proton, such that they might be combined into a single overall factor, large uncertainties on the shape of the reactor antineutrino flux may be expected. On purpose, that is the reason why the near detector JUNO-TAO is going to be built. However, for the scope of the present study, those uncertainties are not expected to have a large impact. Within this assumption, the contributions to the χ^2 function can be represented by a single term as

$$\chi^2_{\text{sys}} = \left(\frac{f^{\text{fit}}_{\text{sys}} - f^{\text{input}}_{\text{sys}}}{\sigma_{f_{\text{sys}}}}\right)^2, \tag{3}$$

where $f^{\text{input}}_{\text{sys}} = 1$ and $\sigma_{f_{\text{sys}}} = 0.03$.

The last term of Equation (1), χ^2_{stat}, represents the statistical fluctuation. When we introduce binning with respect to $E^{\text{obs}}_{\text{vis}}$, it looks like

$$\chi^2_{\text{stat}} = \sum_i \left(\frac{N^{\text{fit}}_i - N^{\text{NH(IH)}}_i}{\sqrt{N^{\text{NH(IH)}}_i}}\right)^2, \tag{4}$$

with the summation running over all the energy bins. Here, $N^{\text{NH(IH)}}_i$ is the event number for the i_{th} bin when the hierarchy is NH(IH). N^{fit}_i is the fitted number of events, calculated

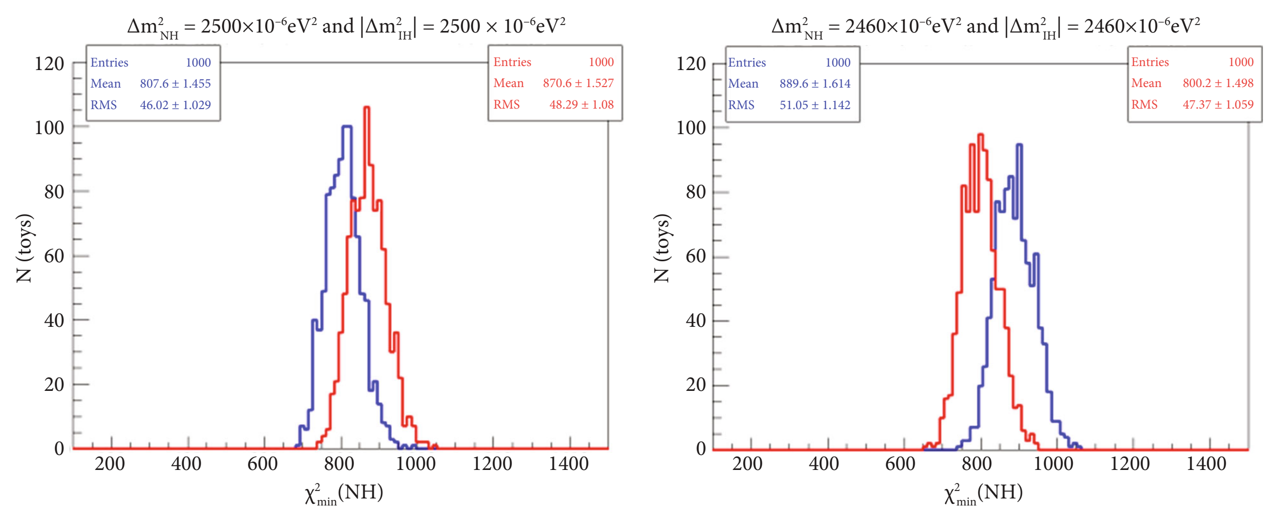

(a) (b)

Figure 1: Two χ^2 distributions for 1000 (NH) + 1000 (IH) toy JUNO-like simulations generated at $\Delta m^2 = 2.500 \times 10^{-3} eV^2$ for (a) NH hypothesis and $\Delta m^2_{input} = -2.460 \times 10^{-3} eV^2$ for (b) IH hypothesis, with six years of exposure and the ten near reactor cores with infinite energy resolution. The intrinsic strong positive correlation between the two components $\chi^2_{min\ (NH)}$ and $\chi^2_{min\ (IH)}$ leads to the overlapping between the two χ^2 distributions.

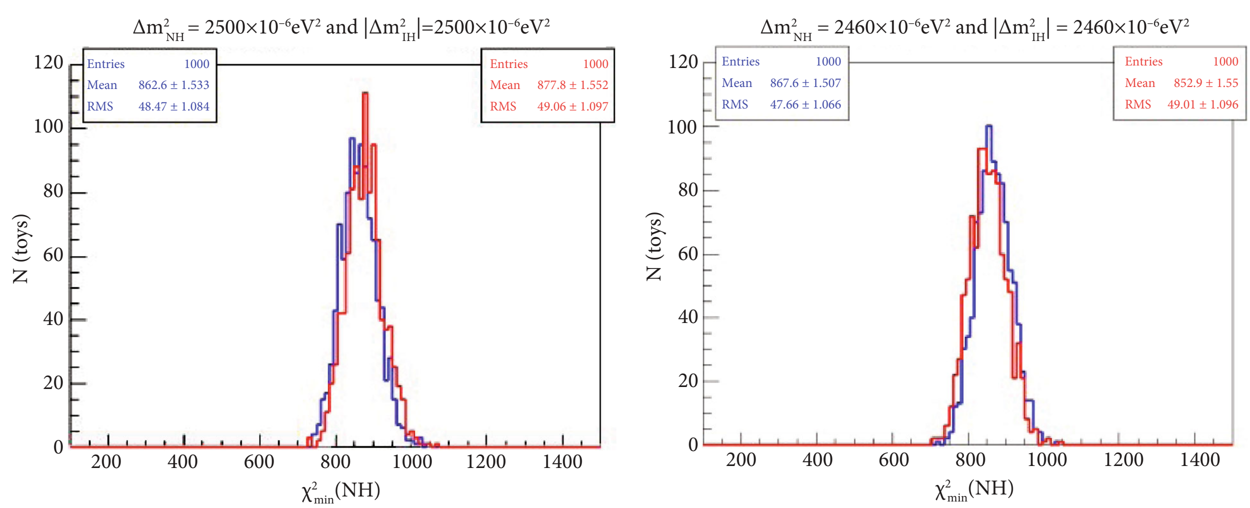

(a) (b)

Figure 2: Two χ^2 distributions for 1000 (NH) + 1000 (IH) toy JUNO-like simulations generated at $\Delta m^2_{input} = 2.500 \times 10^{-3} eV^2$ for (a) NH hypothesis and $\Delta m^2_{input} = -2.460 \times 10^{-3} eV^2$ for (b) IH hypothesis, with six years of exposure and the ten near reactor cores, with 3% relative energy resolution. The intrinsic strong positive correlation between the two components $\chi^2_{min\ (NH)}$ and $\chi^2_{min\ (IH)}$ leads to a very large overlapping between the two χ^2 distributions.

as a function of the four model parameters and the normalization factor f_{sys}. All parameters are varied under the NH(IH) constraints of Equation (2) and Equation (3). A different definition of the χ^2 function based on the Poisson distribution yields a consistent MH sensitivity [8].

In the minimization procedure, all the parameters were initially set to their global best values that are indicated in Table 1. The fitting procedures and the minimization of χ^2 are done with the TMinuit algorithm (ROOT libraries). The χ^2 distributions are obtained for four parameters ($\sin^2\theta_{12}$, $\sin^2\theta_{13}$, δm^2_{sol}, and Δm^2), based on a total of 108357 signal events (Figures 1 and 2).

As reported in [8], the sensitivity can reach $|\Delta\bar{\chi}^2| > 16$ in the ideal case of a single reactor and single detector, and $|\Delta\bar{\chi}^2| > 9$ considering the spread of reactor cores and uncertainties of the detector response. All these results have been reached using semianalytical simulations, i.e., simulations as used in [8, 13]. Semianalytical simulations are generated by fluctuating the bin content according to Poisson or Gaussian distributions that represent the number of events. In addition, a second fluctuation is added by applying $3\%/\sqrt{E}$ energy smearing in each single energy bin and not in each single event. If the energy resolution smearing per each single event is replaced by smearing for the whole bin, an event balance migration occurs, and the number of events per each single bin becomes uncorrelated with side bins leading to the results reported in [8]. We provided the simulation performed on an event–by–event basis and computed the experimental sensitivity for the JUNO by changing the atmospheric neutrino mass. The χ^2 distributions are obtained for $\Delta m^2_{\text{input}} = -2.460 \times 10^{-3}\text{eV}^2$ and $\Delta m^2_{\text{input}} = 2.500 \times 10^{-3}\text{eV}^2$, for IH hypothesis and NH hypothesis, respectively (Figures 1 and 2), with infinite and 3% relative energy resolution, respectively.

3. Issue One: The Limited Power of $\Delta\chi^2$ as a Single-Dimensional Estimator

The two discrete hypotheses are not nested; thus, the Wilks theorem is not applicable in this problem when it is based on the $\Delta\chi^2$ defined in Equation (5). As a consequence, $\Delta\chi^2$ does not follow a χ^2 distribution [14]. The MO significance is usually obtained in terms of the single-dimensional estimator $\Delta\chi^2$, and its evaluation is based on two distinct hypotheses, NH and IH. For each MO, the best solution is found: the $\chi^2_{\min}$ comes from two different best-fit values for the NH model, $\chi^2_{\min\,(\text{NH})}$, and the IH model, $\chi^2_{\min\,(\text{IH})}$:

$$\Delta\chi^2 = \chi^2_{\min\,(\text{NH})} - \chi^2_{\min\,(\text{IH})}, \quad (5)$$

where the two minima are evaluated spanning the uncertainties on the three-neutrino oscillation parameters. The experimental sensitivity to the neutrino mass hierarchy arises from the small phase shift in the oscillation terms depending on the two large mass-squared differences Δm^2_{32} and Δm^2_{31}. JUNO sensitivity can be calculated using the single-dimensional test statistics $\Delta\chi^2$. The median sensitivity can be obtained using the Z-test, where $z^{(\text{NH})}_{\text{score}}$ is the number of σ_{NH} assuming that NH is the true model and $z^{(\text{IH})}_{\text{score}}$ is the number of σ_{IH} assuming that IH is the true model,

$$z^{(\text{NH})}_{\text{score}} = \frac{\left|\overline{\Delta\chi}^{2\,(\text{IH})} - \overline{\Delta\chi}^{2\,(\text{NH})}\right|}{\sigma_{\text{NH}}} \quad z^{(\text{IH})}_{\text{score}} = \frac{\overline{\Delta\chi}^{2\,(\text{NH})} - \overline{\Delta\chi}^{2\,(\text{IH})}}{\sigma_{\text{IH}}}. \quad (6)$$

The $\overline{\Delta\chi}^{2\,(\text{NH})}$, σ_{NH}, $\overline{\Delta\chi}^{2\,(\text{IH})}$, and σ_{IH} are the mean value and standard deviation of the $\Delta\chi^2$ distribution assuming that NH and IH are the true models, respectively. There, an approximation is usually used [8, 15–17]:

Table 2: The comparison of the MH sensitivity at energy resolution $3\%/\sqrt{E}$ for NH sample and IH sample at $|\Delta m^2| = 2.460 \times 10^{-3}\text{eV}^2$ in two cases. The first case makes use of Equation (6), and the second one makes use of Equation (8). The μ_{NH} is the mean value for NH distribution, σ_{NH} is the standard deviation of the NH distribution, μ_{IH} is the mean value for IH distribution, and σ_{IH} is the standard deviation of the IH distribution.

	Energy resolution $3\%/\sqrt{E}$	
μ_{NH}	-15.68 ± 0.85	
σ_{NH}	26.83 ± 0.60	
μ_{IH}	14.75 ± 0.84	
σ_{IH}	26.55 ± 0.60	
$z^{(\text{NH})}_{\text{score}}$	1.134	3.960 (app.)
$z^{(\text{IH})}_{\text{score}}$	1.146	3.841 (app.)

Table 3: The comparison of the MH sensitivity at infinite energy resolution use for NH sample and IH sample at $|\Delta m^2| = 2.460 \times 10^{-3}\text{eV}^2$ in two cases. The first case makes use of Equation (6), and the second one makes use of Equation (8). The μ_{NH} is the mean value for NH distribution, σ_{NH} is the standard deviation of the NH distribution, μ_{IH} is the mean value for IH distribution, and σ_{IH} is the standard deviation of the IH distribution.

	Infinite energy resolution	
μ_{NH}	-59.20 ± 0.79	
σ_{NH}	24.91 ± 0.56	
μ_{IH}	89.41 ± 0.72	
σ_{IH}	22.86 ± 0.51	
$z^{(\text{NH})}_{\text{score}}$	5.966	7.694 (app.)
$z^{(\text{IH})}_{\text{score}}$	6.501	9.456 (app.)

$$\sigma_{\Delta\chi^2} = 2\sqrt{\overline{\Delta\chi}^2}, \quad (7)$$

where $\overline{\Delta\chi}^2$ is the mean value of the $\Delta\chi^2$ distribution. Therefore, Equation (6) becomes

$$z^{(\text{NH})}_{\text{score}} = \sqrt{\left|\overline{\Delta\chi}^{2\,(\text{NH})}\right|} \quad z^{(\text{IH})}_{\text{score}} = \sqrt{\overline{\Delta\chi}^{2\,(\text{IH})}}. \quad (8)$$

When the analysis is performed on an event–by–event basis and not semianalytical simulations as in [8], the dispersions of the distributions cannot be described by Equation (7) anymore. That strongly affects the statistical significance that drops to less than 2σ as indicated in Table 2 for relatively energy resolution and in Table 3 for infinite energy resolution. The reason stays in the convolution of the energy resolution. To check it, the analysis has been also done at an infinite energy resolution to find out whether it is consistent with the latter conclusion (Figure 3).

The investigation of the origin of the approximation has been pursued by looking whether it is still valid in event–by–event simulations as it is in semianalytical simulations. In fact, we found that the dispersion of the two distributions

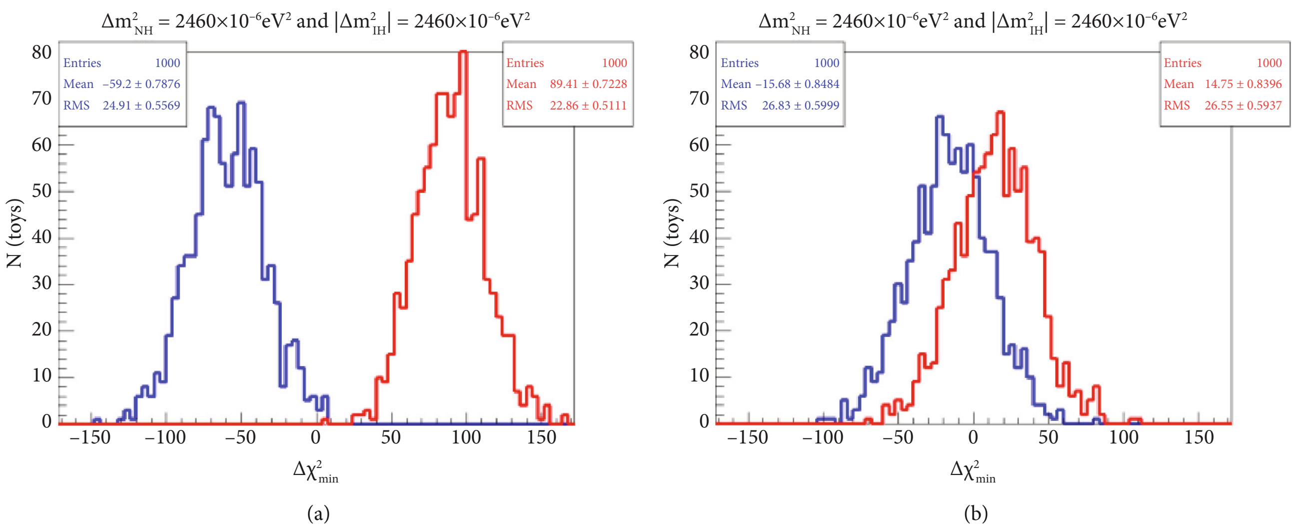

FIGURE 3: $\Delta\chi^2$ estimator for 1000 (NH) + 1000 (IH) toy JUNO-like simulations generated at $|\Delta m^2| = 2.460 \times 10^{-3} eV^2$ for NH and IH hypotheses with six years of exposure and the ten near reactor cores. An infinite energy resolution is assumed for (a) and a 3% relative energy resolution for (b). The experimental sensitivities under these terms are reported in Tables 2 and 3.

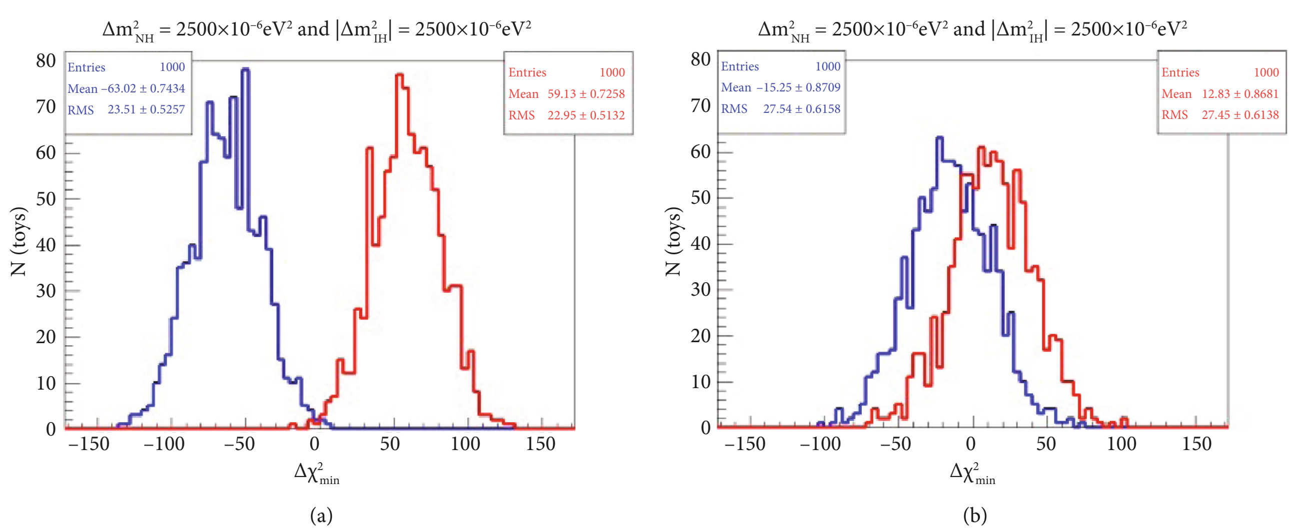

FIGURE 4: $\Delta\chi^2$ estimator for 1000 (NH) + 1000 (IH) toy JUNO-like simulations generated at $|\Delta m^2| = 2.500 \times 10^{-3} eV^2$ for (a) NH hypothesis and (b) IH hypothesis with six years of exposure and the ten near reactor cores. An infinite energy resolution is assumed for the left plot and a 3% relative energy resolution for the right plot. The experimental sensitivities under these terms are reported in Tables 4 and 5, respectively.

becomes wider than in semianalytical simulations when a finite energy resolution is taken into account. The energy error introduces strong correlations between bins, and it corresponds to an extended systematic error.

The limited power of the $\Delta\chi^2$ manifests itself being controlled by the statistical assumption, i.e., Equation (7). The experimental sensitivity is reduced when the energy systematic error is taken into account, and Equation (7) is no more valid. Specific cases are reported in the following figures and tables, and other details are reported in subsection 6.1.

In other words, it is worth to stress the loss of the Gaussianity of the full process. When the energy uncertainty is considered in an event–by–event simulation, a net migration of events occurs from the upper bin to the lower one when the expected number of events is increasing with the energy. The opposite occurs when the event expectation is decreasing with the energy. That corresponds to a loss of independency of the random variables of the energy bin, and a consequent loss of the Gaussianity. Instead, the simple addition of the energy uncertainty in each bin will keep that independence, mystifying the final results.

Figure 4 is a comparison of the $\Delta\chi^2$ estimator distributions at $|\Delta m^2| = 2.500 \times 10^{-3} eV^2$ for NH sample and IH sample. An infinite energy resolution is assumed for the left plot and a 3% relative energy resolution for the right plot.

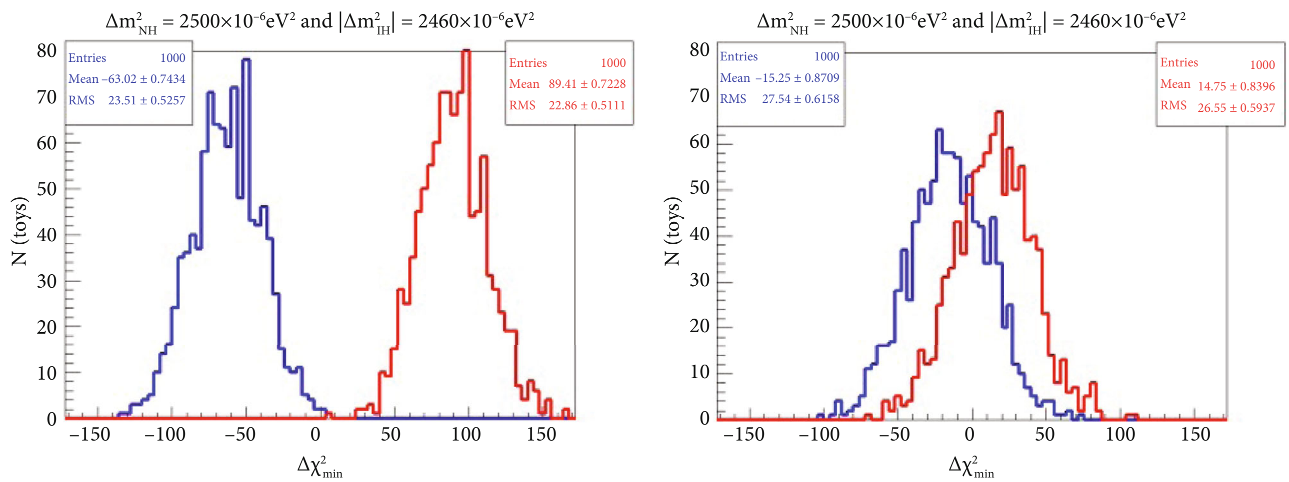

FIGURE 5: $\Delta\chi^2$ estimator for 1000 (NH) + 1000 (IH) toy JUNO-like simulations generated at $\Delta m^2 = 2.500 \times 10^{-3}\text{eV}^2$ for NH hypothesis (blue) and $\Delta m^2 = -2.460 \times 10^{-3}\text{eV}^2$ for IH hypothesis (red) with six years of exposure and the ten near reactor cores. The left plot is for infinite energy resolution, and and the right plot is for 3% relative energy resolution. The experimental sensitivities under these terms are reported in Tables 6 and 7.

Figure 5 for NH sample at $\Delta m^2 = 2.500 \times 10^{-3}\text{eV}^2$ and IH sample for $\Delta m^2 = -2.460 \times 10^{-3}\text{eV}^2$ shows the $\Delta\chi^2$ distributions for a relative 3% and an infinite energy resolution. The JUNO sensitivity is clearly different from that reported in [8].

When only statistical fluctuations are included, the MH sensitivities using Z-test ($z^{(\text{NH})}_{\text{score}}$ and $z^{(\text{IH})}_{\text{score}}$) do not exactly equal to the MH sensitivities obtained in the approximated Equation (7) ($z^{(\text{NH})}_{\text{score}}(\text{app.})$ and $z^{(\text{IH})}_{\text{score}}(\text{app.})$) as reported in Tables 4 and 5. This observation is consistent with what is obtained at the atmospheric mass, $|\Delta m^2| = 2.460 \times 10^{-3}\text{eV}^2$ for IH sample and $\Delta m^2 = 2.500 \times 10^{-3}\text{eV}$ for NH sample for infine energy resolution in Table 6 and for $3\%/\sqrt{E}$ in Table 7. This conclusion will be confirmed for other 18 different values for the atmospheric mass at infinite energy resolution in subsection 6.1.

4. Issue Two: Nonbright Results Using χ^2 as a Bidimensional Estimator

When $\chi^2_{\text{min (IH)}}$ and $\chi^2_{\text{min (NH)}}$ are drawn in a 2D map, their strong positive correlation manifests χ^2 as a bidimensional estimator. This strong positive correlation leads to overlap between the χ^2 distributions of the two hypotheses, thus reducing the experiment sensitivity. When we look at χ^2 as a bidimensional estimator, the experiment sensitivity can be calculated with a Z-test for two-dimensional test statistic providing the results indicated in Tables 8, 9, and 10.

Using Z-test for 2D, the MH sensitivity can be calculated as

$$z^{(\text{NH})}_{\text{score}} = \frac{\sqrt{\left(\bar{\chi}^{2\,(\text{NH})}_{\text{IH}} - \bar{\chi}^{2\,(\text{IH})}_{\text{IH}}\right)^2 + \left(\bar{\chi}^{2\,(\text{NH})}_{\text{NH}} - \bar{\chi}^{2\,(\text{IH})}_{\text{NH}}\right)^2}}{\sqrt{\left(\sigma^2_{\text{IH}}\right)^{\text{NH}} + \left(\sigma^2_{\text{NH}}\right)^{\text{NH}}}},$$

$$z^{(\text{IH})}_{\text{score}} = \frac{\sqrt{\left(\bar{\chi}^{2\,(\text{IH})}_{\text{IH}} - \bar{\chi}^{2\,(\text{NH})}_{\text{IH}}\right)^2 + \left(\bar{\chi}^{2\,(\text{IH})}_{\text{NH}} - \bar{\chi}^{2\,(\text{NH})}_{\text{NH}}\right)^2}}{\sqrt{\left(\sigma^2_{\text{IH}}\right)^{\text{IH}} + \left(\sigma^2_{\text{NH}}\right)^{\text{IH}}}}. \quad (9)$$

$\bar{\chi}^{2\,(A)}_{B}$, where A, B = NH, IH, indicates the mean of the χ^2 distribution of the A sample, assuming the B hypothesis to be true. $(\sigma^2_B)^A$ expresses the standard derivation of χ^2 distribution of the A sample assuming that B hypothesis is the true hypothesis. Figures 6–8 are shown the 2D maps.

5. Issue Three: The Robustness

Robust statistics are the statistics that yield good performance when data is drawn from a wide range of probability distributions that are largely unaffected by outliers or small departures from model assumptions in a given data set [18]. In other words, a robust statistic is resistant to initial deviations with respect to the final results [19].

The main focus of the statistical analysis using the $\Delta\chi^2$ standard method is to calculate neutrino mass hierarchy determination sensitivity, and less attention or none is put about its robustness. Subsection 5.1 will discuss how the standard method using $\Delta\chi^2$ is not able to maintain the robustness while subsection 5.2 will discuss the inability of the χ^2 to establish the robustness as a bidimensional estimator. This study is done for 20 different data values of the input atmospheric neutrino mass in the range, $2.450 \times 10^{-3}\text{eV}^2 \leq |\Delta m^2|_{\text{input}} \leq 2.580 \times 10^{-3}\text{eV}^2$.

5.1. The $|\overline{\Delta\chi^2}|$ Oscillations with Δm^2_{input}. There are trends in our data to confirm that the $|\overline{\Delta\chi^2}|$ varies with the input atmospheric neutrino mass $|\Delta m^2|_{\text{input}}$. We studied the

Table 4: The comparison of the MH sensitivity for ideal distributions for NH sample and IH sample at $|\Delta m^2| = 2.500 \times 10^{-3}\text{eV}^2$ in two cases. The first case makes use of Equation (6), and the second one makes use of Equation (8). The μ_{NH} is the mean value for NH distribution, σ_{NH} is the standard deviation of the NH distribution, μ_{IH} is the mean value for IH distribution, and σ_{IH} is the standard deviation of the IH distribution.

	Infinite energy resolution	
μ_{NH}	-63.02 ± 0.74	
σ_{NH}	23.51 ± 0.53	
μ_{IH}	59.13 ± 0.73	
σ_{IH}	22.95 ± 0.51	
$z_{\text{score}}^{(\text{NH})}$	5.203	7.950 (app.)
$z_{\text{score}}^{(\text{IH})}$	5.330	7.690 (app.)

Table 5: The comparison of the MH sensitivity for actual distributions for NH sample and IH sample at $|\Delta m^2| = 2.500 \times 10^{-3}\text{eV}^2$ in two cases. The first case makes use of Equation (6), and the second one makes use of Equation (8).The μ_{NH} is the mean value for NH distribution, σ_{NH} is the standard deviation of the NH distribution, μ_{IH} is the mean value for IH distribution, and σ_{IH} is the standard deviation of the IH distribution.

	$3\%/\sqrt{E}$ energy resolution	
μ_{NH}	-15.25 ± 0.87	
σ_{NH}	27.54 ± 0.62	
μ_{IH}	12.83 ± 0.87	
σ_{IH}	27.45 ± 0.61	
$z_{\text{score}}^{(\text{NH})}$	1.020	3.901 (app.)
$z_{\text{score}}^{(\text{IH})}$	1.023	3.582 (app.)

Table 6: The comparison of the MH sensitivity for ideal distributions for NH sample at $\Delta m^2 = 2.500 \times 10^{-3}\text{eV}^2$ and IH sample for $\Delta m^2 = -2.460 \times 10^{-3}\text{eV}^2$ in two cases. The first case makes use of Equation (6), and the second one makes use of Equation (8). The μ_{NH} is the mean value for NH distribution, σ_{NH} is the standard deviation of the NH distribution, μ_{IH} is the mean value for IH distribution, and σ_{IH} is the standard deviation of the IH distribution.

	Infinite energy resolution	
μ_{NH}	-63.02 ± 0.74	
σ_{NH}	23.51 ± 0.53	
μ_{IH}	89.41 ± 0.72	
σ_{IH}	22.86 ± 0.51	
$z_{\text{score}}^{(\text{NH})}$	6.484	7.950 (app.)
$z_{\text{score}}^{(\text{IH})}$	6.668	9.456 (app.)

Table 7: The comparison of the MH sensitivity for actual distributions for NH sample at $\Delta m^2 = 2.500 \times 10^{-3}\text{eV}^2$ and IH sample for $\Delta m^2 = -2.460 \times 10^{-3}\text{eV}^2$ in two cases. The first case makes use of Equation (6), and the second one makes use of Equation (8). The μ_{NH} is the mean value for NH distribution, σ_{NH} is the standard deviation of the NH distribution, μ_{IH} is the mean value for IH distribution, and σ_{IH} is the standard deviation of the IH distribution.

	$3\%/\sqrt{E}$ energy resolution	
μ_{NH}	-15.25 ± 0.87	
σ_{NH}	27.54 ± 0.62	
μ_{IH}	14.75 ± 0.84	
σ_{IH}	26.55 ± 0.60	
$z_{\text{score}}^{(\text{NH})}$	1.089	3.960 (app.)
$z_{\text{score}}^{(\text{IH})}$	1.130	3.841 (app.)

relation between the $|\overline{\Delta\chi^2}|$ values and the value of the input parameter for 20 different values, $|\Delta m^2|_{\text{input}}$ in the range, $2.450 \times 10^{-3}\text{eV}^2 \leq |\Delta m^2|_{\text{input}} \leq 2.580 \times 10^{-3}\text{eV}^2$, and we computed the corresponding experimental sensitivity for the two cases, with and without including the systematic uncertainties. In particular, since the main systematic error is largely dominated by the energy resolution, when we refer to with/without systematics, we are either taking into account or not the systematic uncertainty due to the energy resolution, which is taken to be 3%. Figure 9 illustrates the variation of $|\overline{\Delta\chi^2}|$ as a function of the input atmospheric neutrino mass $|\Delta m^2|_{\text{input}}$, in the range of $2.450 \times 10^{-3}\text{eV}^2 \leq |\Delta m^2|_{\text{input}} \leq 2.580 \times 10^{-3}\text{eV}^2$, assuming infinite energy resolution. Figure 10 illustrates the variation of $\Delta\chi^2$ with the input atmospheric neutrino mass $|\Delta m^2|_{\text{input}}$, in the range of $2.450 \times 10^{-3}\text{eV}^2 \leq |\Delta m^2|_{\text{input}} \leq 2.580 \times 10^{-3}\text{eV}^2$ when the 3% relative energy resolution is included. We performed additional data collection ignoring the systematic uncertainties in order to provide a strong evidence for the result. How the $|\overline{\Delta\chi^2}|$ oscillations with $\Delta m^2_{\text{input}}$ reflects on the neutrino mass hierarchy determination sensitivity depends on how the significance will be calculated, for example using Equation (6) or Equation (8).

In case the approximation is not valid, the Z-test for 1D, sigmaIH, can be used to calculate the neutrino MH sensitivity. As expected, the variation of the estimator $|\overline{\Delta\chi^2}|$ will influence neutrino MH sensitivity. Figure 11 confirms the influence on neutrino MH sensitivity in case that only the statistical uncertainties are included and the sensitivity varies from about 4.5σ to 7.5σ. Figure 12 confirms this influence in case that the systematic and statistical uncertainties are included and the sensitivity oscillates from about 0.9σ to 1.5σ.

Assuming that the approximation of Equation (7) is valid at infinite energy resolution, the neutrino mass hierarchy determination sensitivity is expected to have a large variation with the input parameter as confirmed in Figure 13. The sensitivity may vary from about 9.5σ to 7.5σ.

Table 8: Two χ^2 distributions for 1000 (NH) + 1000 (IH) toy JUNO-like simulations generated at $|\Delta m^2| = 2.460 \times 10^{-3}\mathrm{eV}^2$ for NH and IH hypotheses with six years of exposure and the ten near reactor cores. The sensitivity is calculated using Equation (9). The μ_{NH} is the mean value for NH distribution, σ_{NH} is the standard deviation of the NH distribution, μ_{IH} is the mean value for IH distribution, and σ_{IH} is the standard deviation of the IH distribution.

Energy resolution	Infinite		3%	
	NH	IH	NH	IH
μ_{NH}	810.7 ± 1.53	889.6 ± 1.61	860.10 ± 1.56	867.60 ± 1.51
σ_{NH}	48.48 ± 1.08	51.05 ± 1.14	49.39 ± 1.10	47.67 ± 1.06
μ_{IH}	869.8 ± 1.63	800.2 ± 1.50	875.80 ± 1.54	852.9 ± 1.55
σ_{IH}	51.57 ± 1.15	47.30 ± 1.06	48.77 ± 1.09	49.03 ± 1.10
$z_{\mathrm{score}}^{(\mathrm{NH})}$	1.072σ		0.219σ	
$z_{\mathrm{score}}^{(\mathrm{IH})}$	1.089σ		0.223σ	

Table 9: Two χ^2 distributions for 1000(NH) + 1000 (IH) toy JUNO-like simulations generated at $|\Delta m^2| = 2.500 \times 10^{-3}\mathrm{eV}^2$ for NH and IH hypotheses with six years of exposure and ten near reactor cores. The sensitivity is calculated using Equation (9). The μ_{NH} is the mean value for NH distribution, σ_{NH} is the standard deviation of the NH distribution, μ_{IH} is the mean value for IH distribution, and σ_{IH} is the standard deviation of the IH distribution.

	Infinite		3%	
	NH	IH	NH	IH
μ_{NH}	807.6 ± 1.46	865.30 ± 1.52	862.60 ± 1.53	870.20 ± 1.60
σ_{NH}	46.05 ± 1.03	48.12 ± 1.08	48.49 ± 1.08	50.58 ± 1.13
μ_{IH}	870.60 ± 1.53	806.20 ± 1.48	877.80 ± 1.55	857.4 ± 1.58
σ_{IH}	48.34 ± 1.08	46.91 ± 1.05	49.04 ± 1.10	49.90 ± 1.12
$z_{\mathrm{score}}^{(\mathrm{NH})}$	0.916σ		0.204σ	
$z_{\mathrm{score}}^{(\mathrm{IH})}$	0.910σ		0.200σ	

Table 10: Two χ^2 distributions for 1000 (NH) + 1000 (IH) toy JUNO-like simulations generated at $\Delta m^2 = 2.500 \times 10^{-3}\mathrm{eV}^2$ for NH hypothesis and $\Delta m^2 = -2.460 \times 10^{-3}\mathrm{eV}^2$ for IH hypothesis with six years of exposure and ten near reactor cores. The sensitivity is calculated using Equation (9). The μ_{NH} is the mean value for NH distribution, σ_{NH} is the standard deviation of the NH distribution, μ_{IH} is the mean value for IH distribution, and σ_{IH} is the standard deviation of the IH distribution.

	Infinite		3%	
	NH	IH	NH	IH
μ_{NH}	807.6 ± 1.46	889.6 ± 1.61	862.60 ± 1.53	867.6 ± 1.51
σ_{NH}	46.05 ± 1.03	51.05 ± 1.14	48.49 ± 1.08	47.67 ± 1.07
μ_{IH}	870.60 ± 1.53	800.2 ± 1.50	877.80 ± 1.55	852.90 ± 1.55
σ_{IH}	48.34 ± 1.08	47.30 ± 1.06	49.04 ± 1.08	49.03 ± 1.07
$z_{\mathrm{score}}^{(\mathrm{NH})}$	1.159σ		0.217σ	
$z_{\mathrm{score}}^{(\mathrm{IH})}$	1.113σ		0.219σ	

Assuming that the approximation of Equation (7) is still valid at 3% relative energy resolution, the neutrino mass hierarchy determination sensitivity is not robust as confirmed in Figure 14. The sensitivity using Equation (8) varies from a maximum of 4.1σ to about 3.2σ.

5.2. The χ^2 Robustness. The significance using χ^2 as bidimensional distribution through Equation (9) varies from 1.3σ to 0.9σ assuming an infinite energy resolution as shown in Figure 15 and from 0.24σ to 0.18σ assuming 3% relative energy resolution, as shown in Figure 16.

The oscillation of the experimental sensitivity with the value of the input parameter, the neutrino atmospheric mass difference ($|\Delta m^2|_{\mathrm{input}}$), implies that the standard method results have a strong dependency on the input parameter value. Whether the approximation is not valid or not, systematic uncertainties included or not, this dependence still holds.

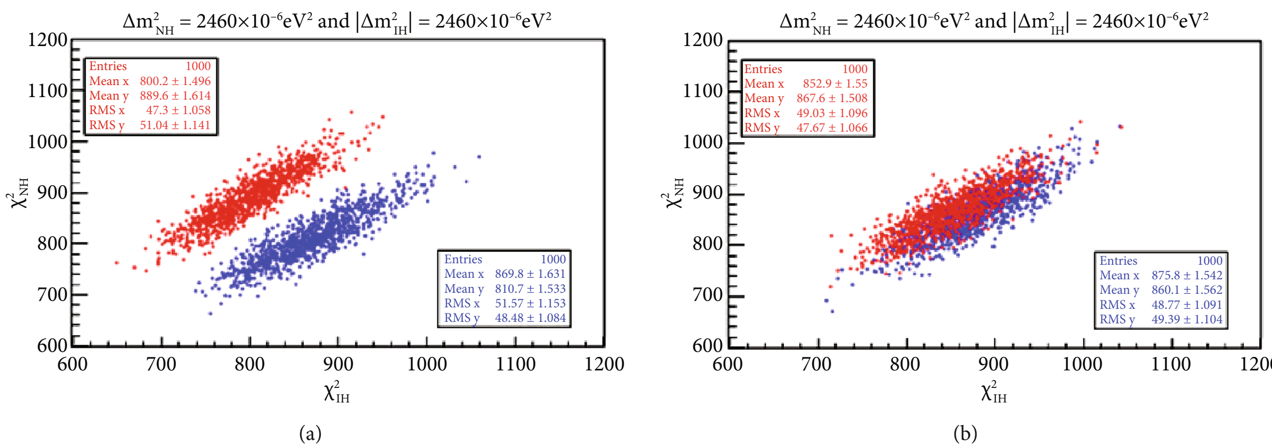

Figure 6: Two islands of χ^2 for 1000 (NH) + 1000 (IH) toy JUNO-like simulations generated at $|\Delta m^2| = 2.460 \times 10^{-3}\text{eV}^2$ for NH hypothesis (blue color) and IH hypothesis (red color) with six years of exposure and the ten near reactor cores. An infinite energy resolution is assumed for (a) and $3\%/\sqrt{E}$ energy resolution for (b). The experimental sensitivities under these terms are reported in Table 8.

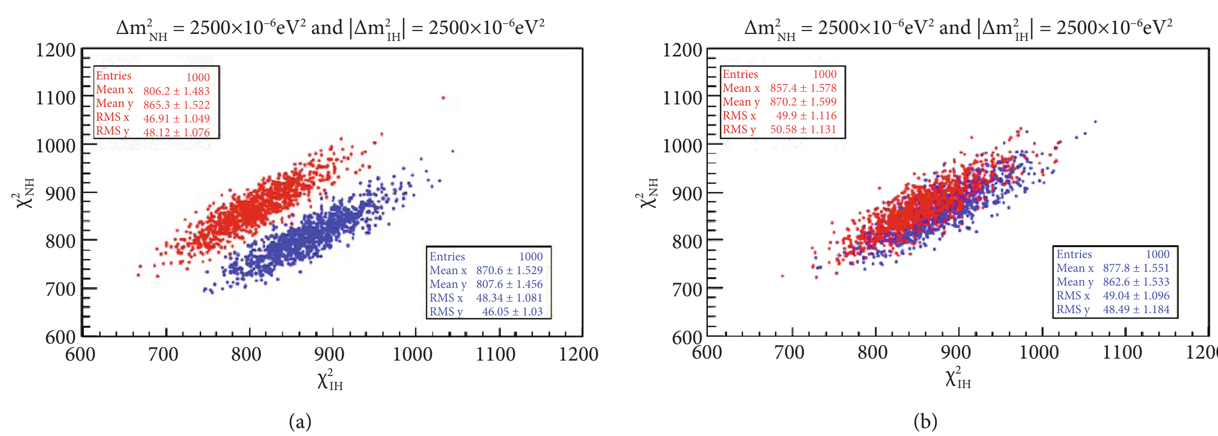

Figure 7: Two islands of χ^2 for 1000(NH) + 1000 (IH) toy JUNO-like simulations generated at $|\Delta m^2| = 2.500 \times 10^{-3}\text{eV}^2$ for NH hypothesis (blue island) and IH hypothesis (red island) with six years of exposure and the ten near reactor cores. An infinite energy resolution is assumed for (a) and a 3% relative energy resolution for (b). The experimental sensitivities under these terms are reported in Table 9.

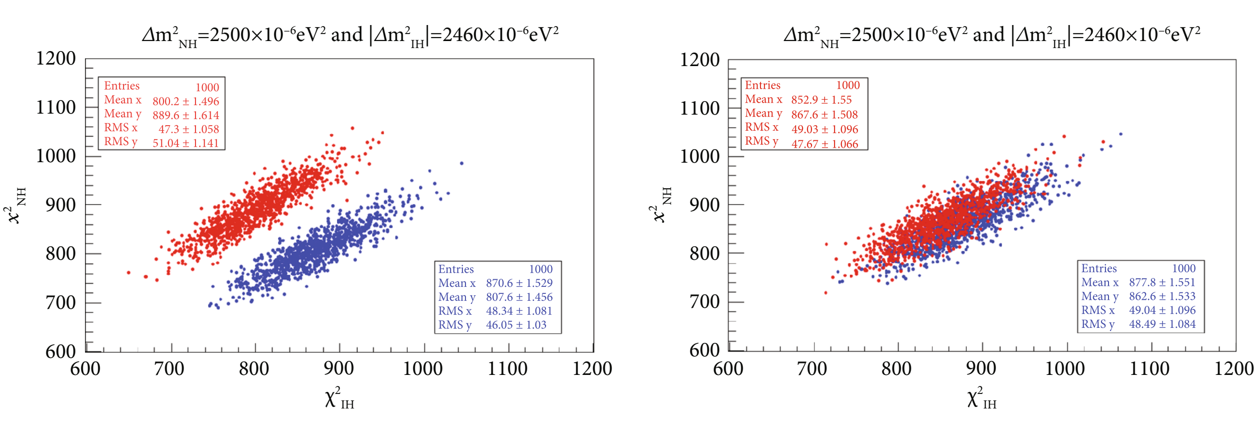

Figure 8: Two islands of χ^2 for 1000 (NH) + 1000 (IH) toy JUNO-like simulations generated at $\Delta m^2 = 2.500 \times 10^{-3}\text{eV}^2$ for NH hypothesis (blue island) and $\Delta m^2 = -2.460 \times 10^{-3}\text{eV}^2$ for IH hypothesis (red island) with six years of exposure and the ten near reactor cores. An infinite energy resolution is assumed for (a) and a 3% relative energy resolution for (b). The experimental sensitivities under these terms are reported in Table 10.

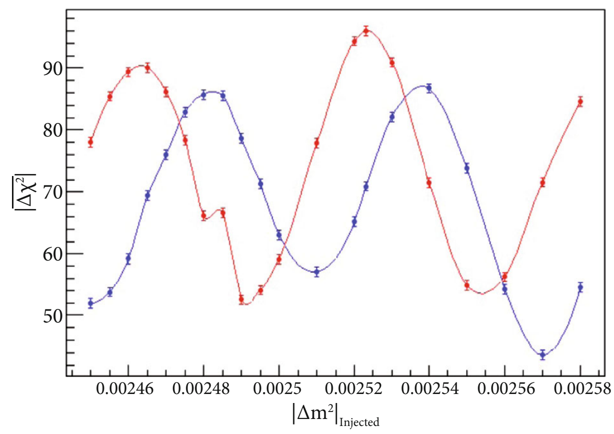

Figure 9: $|\bar{\Delta\chi}^2|$ variation with $|\Delta m^2|_{\text{injected}}$ in the range of $2.450 \times 10^{-3}\text{eV}^2 \leq |\Delta m^2|_{\text{injected}} \leq 2.580 \times 10^{-3}\text{eV}^2$ for 1000 (NH) + 1000 (IH) toy JUNO-like simulations for each point of $|\Delta m^2|_{\text{input}}$ with six years of exposure and the ten near reactor cores assuming an infinite energy resolution. The error bars correspond to the standard error of the $|\bar{\Delta\chi}^2|$ that is calculated as the standard deviation of the $\Delta\chi^2$ distribution divided by the square root of the sample size.

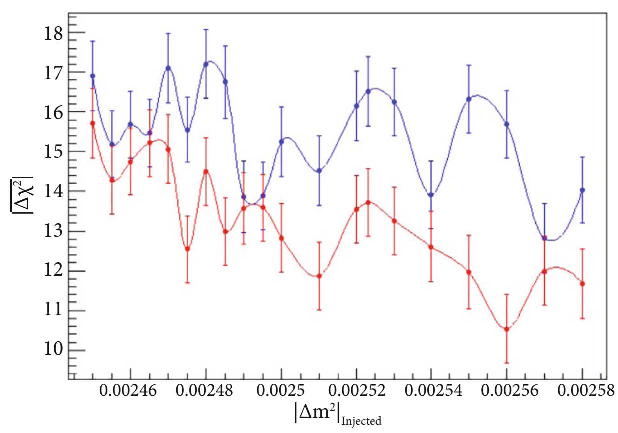

Figure 10: $|\bar{\Delta\chi}^2|$ varies with $|\Delta m^2|_{\text{injected}}$ in the range of $2.450 \times 10^{-3}\text{eV}^2 \leq |\Delta m^2| \leq 2.580 \times 10^{-3}\text{eV}^2$ for 1000 (NH) + 1000 (IH) toy JUNO-like simulations for each point of $|\Delta m^2|_{\text{injected}}$ with six years of exposure and the ten near reactor cores assuming 3% relative energy resolution. The error bars correspond to the standard error of the $|\bar{\Delta\chi}^2|$ that is calculated as the standard deviation of the $\Delta\chi^2$ distribution divided by the square root of the sample size.

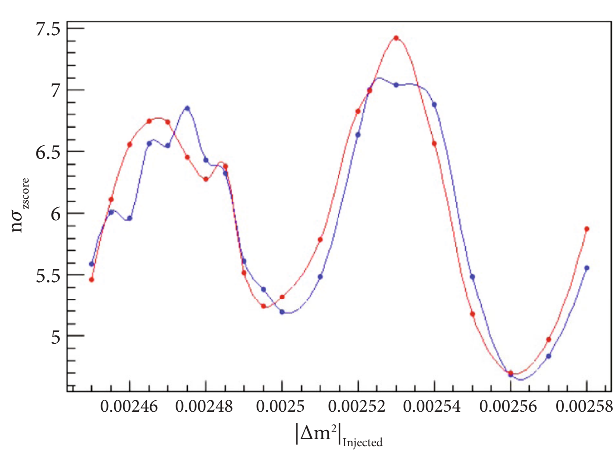

Figure 11: The oscillation of significance with $|\Delta m^2|_{\text{injected}}$ in the range of $2.450 \times 10^{-3}\text{eV}^2 \leq |\Delta m^2| \leq 2.580 \times 10^{-3}\text{eV}^2$ for 1000 (NH) + 1000 (IH) JUNO-toy-like simulations for one benchmark assuming an infinite energy resolution where the blue line is for NH sample and the red line is for IH sample. The sensitivity using Equation (6) varies from about 4.5σ to 7.5σ.

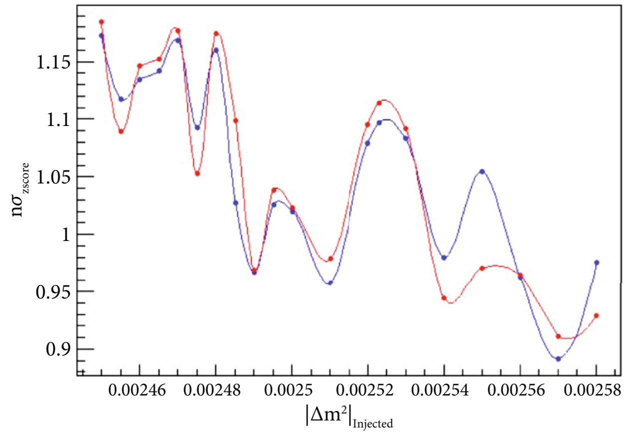

Figure 12: The variation of significance with $|\Delta m^2|_{\text{injected}}$ in the range of $2.450 \times 10^{-3}\text{eV}^2 \leq |\Delta m^2| \leq 2.580 \times 10^{-3}\text{eV}^2$ for 1000 (NH) + 1000 (IH) JUNO-toy-like simulations for one benchmark assuming $3\%/\sqrt{E}$ energy resolution where the blue line is for NH sample and the red line is for IH sample. The sensitivity using the sigmaIH oscillates from about 0.9σ to 1.5σ.

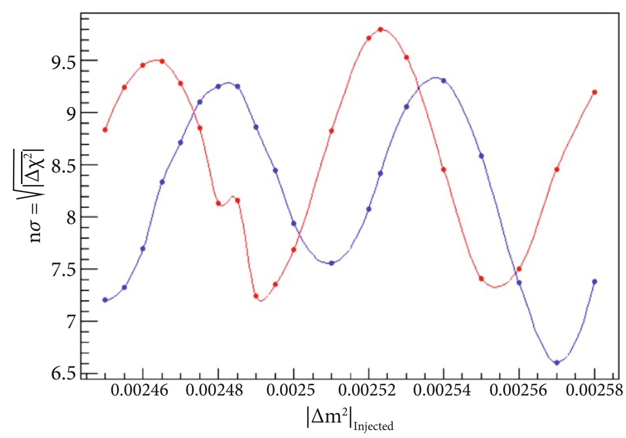

Figure 13: The oscillation of significance with $|\Delta m^2|_{\text{injected}}$ in the range of $2.450 \times 10^{-3}\text{eV}^2 \leq |\Delta m^2| \leq 2.580 \times 10^{-3}\text{eV}^2$ for 1000 (NH) + 1000 (IH) JUNO-toy-like simulations for one benchmark assuming an infinite energy resolution where the blue line is for NH sample and the red line is for IH sample. The sensitivity using Equation (8) varies from about 6.5σ to 9.5σ.

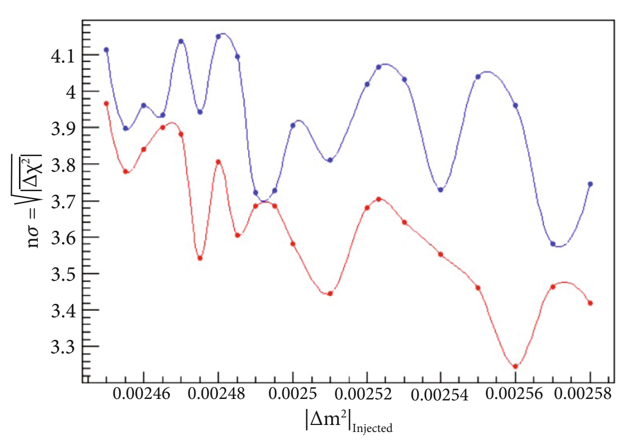

Figure 14: The variation of significance with $|\Delta m^2|_{\text{injected}}$ in the range of $2.450 \times 10^{-3}\text{eV}^2 \leq |\Delta m^2| \leq 2.580 \times 10^{-3}\text{eV}^2$ for 1000 (NH) + 1000 (IH) JUNO-toy-like simulations for one benchmark assuming $3\%/\sqrt{E}$ energy resolution where the blue line is for NH sample and the red line is for IH sample. The sensitivity using the zScorIH varies from about 3.2σ to 4.1σ.

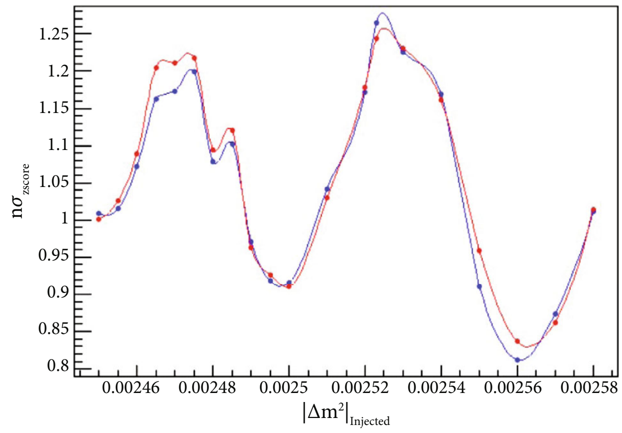

Figure 15: The oscillation of significance using χ^2 as bidimensional distribution through Equation (9) with $|\Delta m^2|_{\text{injected}}$ in the range of $2.450 \times 10^{-3}\text{eV}^2 \leq |\Delta m^2| \leq 2.580 \times 10^{-3}\text{eV}^2$ for 1000 (NH) + 1000 (IH) JUNO-toy-like simulations for one benchmark assuming an infinite energy resolution where the blue line is for NH sample and the red line is for IH sample. The significance varies from about 0.8σ to 1.3σ.

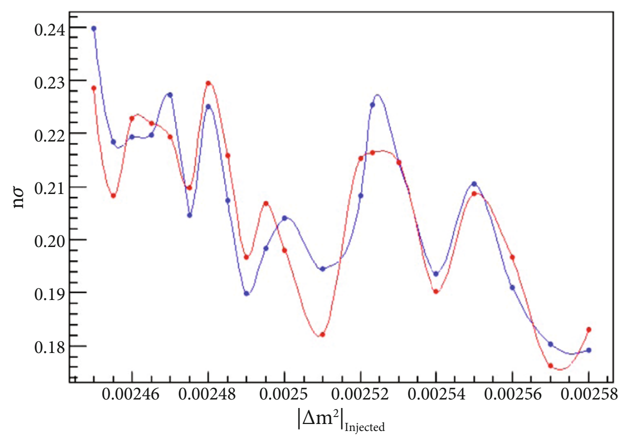

Figure 16: The oscillation of the experimental significance using χ^2 as bidimensional distribution with $|\Delta m^2|_{\text{injected}}$ in the range of $2.450 \times 10^{-3}\text{eV}^2 \leq |\Delta m^2| \leq 2.580 \times 10^{-3}\text{eV}^2$ for 1000 (NH) + 1000 (IH) JUNO-toy-like simulations for one benchmark assuming a 3% relative energy resolution where the blue line is for NH sample and the red line is for IH sample. The significance using Equation (9) varies from about 0.175σ to 0.24σ.

6. Results

In order to present the findings as clear as possible, it is imperative to study the three reported issues of the standard algorithm in the range of the atmospheric mass between 2.450×10^{-3} eV^2 and 2.580×10^{-3} eV^2. These issues are categorized into two types depending on which estimator is being used. The first sensitivity category using $\boldsymbol{\Delta\chi^2}$ estimator is reported in subsection 6.1. The second sensitivity category using χ^2 is reported in subsection 6.2. For each category, a detailed study is provided for 20 different values of the atmospheric mass in the range of $\mathbf{2.450 \times 10^{-3}eV^2 \leq |\Delta m^2|_{input} \leq 2.580 \times 10^{-3}eV^2}$, with and without systematic errors. The final results now provide solid evidences about the problematic use of the standard algorithm.

6.1. The Issues of $\Delta\chi^2$. Here, we report two results. First, our result on the limited power of $\Delta\chi^2$ (issue one) confirming that, when systematic uncertainties are included, the approximated Equation (7) is not acceptable in the range of neutrino atmospheric mass, $2.450 \times 10^{-3}\text{eV}^2 \leq |\Delta m^2|_{\text{input}} \leq 2.580 \times 10^{-3}\text{eV}^2$. We provide the results of 20 different values of the $|\Delta m^2|_{\text{input}}$ in that range showing the limit of the approximation when including the systematic uncertainties (as confirmed in Figure 17). Although Equation (7) is widely accepted, it suffers from some limitations due to its limitation when systematic uncertainties are included (Figure 17). The limitation manifests itself decreasing the power of the $\Delta\chi^2$ estimator to determine the correct neutrino MH. The reasons behind this limitation are explained in details in Section 3. As a result, the power of this estimator

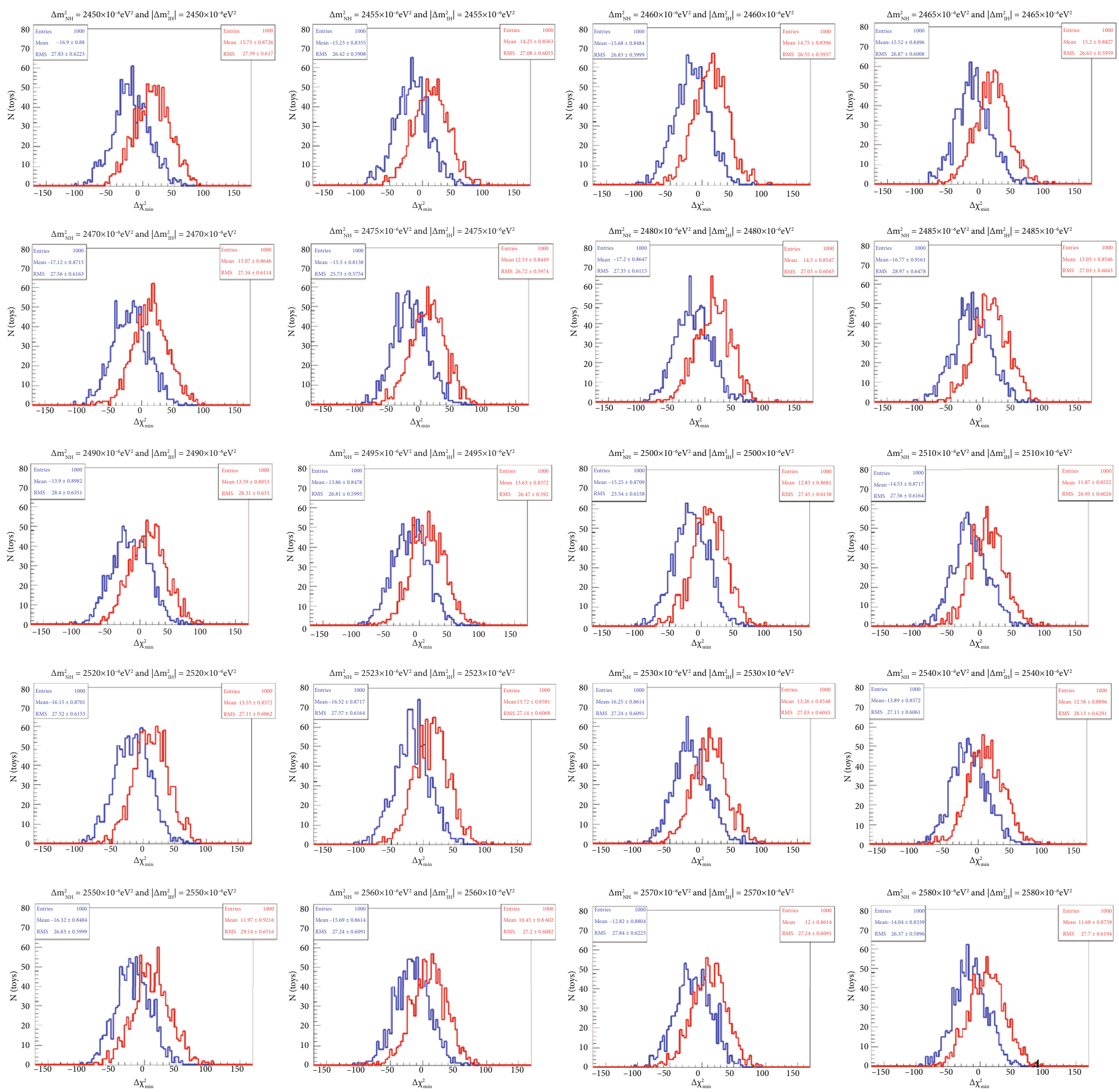

FIGURE 17: $\Delta\chi^2$ estimator for 1000 (NH) + 1000 (IH) toy JUNO-like simulations generated at 20 different values of the atmospheric mass in the range of $2.450 \times 10^{-3}\text{eV}^2 \leq |\Delta m^2| \leq 2.580 \times 10^{-3}\text{eV}^2$ for NH hypothesis (blue distribution in each plot) and IH hypothesis (red distribution in each plot) with six years of exposure and the ten near reactor cores, with energy resolution $3\%/\sqrt{E}$. The sensitivities due to these conditions are reported in Table 11.

for the MH discrimination is not promising as reported in Table 11. On the contrary, without including the systematic uncertainties, Equation (7) is valid, and the $\Delta\chi^2$ results are very good as reported in Figure 18 and Table 12. Second, the studies about the $\Delta\chi^2$ robustness in the range of $2.450 \times 10^{-3}\text{eV}^2 \leq |\Delta m^2|_{\text{input}} \leq 2.580 \times 10^{-3}\text{eV}^2$ show its dependence. This result is directly in line with previous result in Section 5. From these sensitivity tables, (Tables 11 and 12), it is clear that the experimental sensitivity using $\Delta\chi^2$ has a strong dependence on the value of the input atmospheric mass. If the value of the input parameter, input atmospheric mass, is modified, the experimental sensitivity will change according to it. This change is not affected by the systematic uncertainties. It is an intrinsic property of the $\Delta\chi^2$ itself. Table 12 shows the sensitivities using $\Delta\chi^2$ with infinite energy resolution. As can be seen in the table, the experimental sensitivities vary a lot with different values of the neutrino atmospheric mass proving that the robustness of $\Delta\chi^2$ is not well established even at infinite energy resolution. Table 11 provides the sensitivities including the systematic uncertainties: the neutrino mass ordering discrimination varies a lot. The implications of this issue are fully discussed in Section 5.

Table 11: The comparison of the MH sensitivity using $\Delta\chi^2$ for actual distributions for NH sample and IH sample, for 20 different values of the atmospheric mass in the range of $2.450 \times 10^{-3} \text{eV}^2 \leq |\Delta m^2| \leq 2.580 \times 10^{-3} \text{eV}^2$. The table indicates the sensitivity calculations using the Z-test for the 1D test in two cases. The first case is without the approximation of Equation (7), and the second one is using the approximation of Equation (7).

Relative energy resolution $3\%/\sqrt{E}$								
$\left\|\Delta m^2\right\|_{NH/IH} \times 10^{-3}$	2.450		2.455		2.460		2.465	
μ_{NH}	-16.91 ± 0.880		-15.19 ± 0.834		-15.68 ± 0.8484		-15.48 ± 0.85	
σ_{NH}	27.82 ± 0.622		26.38 ± 0.590		26.83 ± 0.5999		26.88 ± 0.601	
μ_{IH}	15.72 ± 0.871		14.29 ± 0.856		14.75 ± 0.8396		15.22 ± 0.8427	
σ_{IH}	27.55 ± 0.616		27.06 ± 0.605		26.55 ± 0.5937		26.65 ± 0.5959	
$z_{score}^{(NH)}$	1.173	4.112 (app.)	1.118	3.897 (app.)	1.134	3.960 (app.)	1.142	3.934 (app.)
$z_{score}^{(IH)}$	1.184	3.965 (app.)	1.089	3.780 (app.)	1.146	3.841 (app.)	1.152	3.901 (app.)
$\left\|\Delta m^2\right\|_{NH/IH} \times 10^{-3}$	2.470		2.475		2.480		2.485	
μ_{NH}	-17.10 ± 0.8709		-15.55 ± 0.8126		-17.21 ± 0.8646		-16.76 ± 0.9159	
σ_{NH}	27.54 ± 0.6158		25.70 ± 0.5746		27.34 ± 0.6114		28.96 ± 0.6477	
μ_{IH}	15.07 ± 0.8645		12.54 ± 0.8437		14.49 ± 0.8539		12.99 ± 0.856	
σ_{IH}	27.34 ± 0.6113		26.68 ± 0.5966		27.00 ± 0.6038		27.07 ± 0.6053	
$z_{score}^{(NH)}$	1.168	4.135 (app.)	1.093	3.943 (app.)	1.159	4.148 (app.)	1.027	4.094 (app.)
$z_{score}^{(IH)}$	1.177	3.882 (app.)	1.053	3.541 (app.)	1.174	3.807 (app.)	1.099	3.604 (app.)
$\left\|\Delta m^2\right\|_{NH/IH} \times 10^{-3}$	2.490		2.495		2.500		2.510	
μ_{NH}	-13.86 ± 0.8974		-13.89 ± 0.8476		-15.25 ± 0.8709		14.52 ± 0.871	
σ_{NH}	28.38 ± 0.6345		26.80 ± 0.5994		27.54 ± 0.6158		27.55 ± 0.616	
μ_{IH}	13.58 ± 0.8955		13.59 ± 0.8372		12.83 ± 0.8681		11.87 ± 0.853	
σ_{IH}	28.32 ± 0.6332		26.47 ± 0.5920		27.45 ± 0.6138		26.97 ± 0.603	
$z_{score}^{(NH)}$	0.967	3.723 (app.)	1.025	3.727 (app.)	1.020	3.905 (app.)	0.958	3.811 (app.)
$z_{score}^{(IH)}$	0.969	3.685 (app.)	1.038	3.686 (app.)	1.023	3.582 (app.)	0.978	3.445 (app.)
$\left\|\Delta m^2\right\|_{NH/IH} \times 10^{-3}$	2.520		2.523		2.530		2.540	
μ_{NH}	-16.15 ± 0.870		-16.52 ± 0.872		-16.25 ± 0.861		-13.91 ± 0.856	
σ_{NH}	27.52 ± 0.615		27.57 ± 0.616		27.24 ± 0.609		27.07 ± 0.605	
μ_{IH}	13.55 ± 0.857		13.72 ± 0.858		13.26 ± 0.855		12.61 ± 0.888	
σ_{IH}	27.11 ± 0.606		27.14 ± 0.607		27.03 ± 0.605		28.08 ± 0.628	
$z_{score}^{(NH)}$	1.079	4.019 (app.)	1.097	4.064 (app.)	1.083	4.031 (app.)	0.9797	3.30 (app.)
$z_{score}^{(IH)}$	1.096	3.681 (app.)	1.114	3.704 (app.)	1.092	3.641 (app.)	0.944	3.551 (app.)
$\left\|\Delta m^2\right\|_{NH/IH} \times 10^{-3}$	2.550		2.560		2.570		2.580	
μ_{NH}	-16.32 ± 0.848		-15.69 ± 0.861		-12.82 ± 0.880		-14.04 ± 0.834	
σ_{NH}	26.83 ± 0.600		27.24 ± 0.609		27.84 ± 0.623		26.37 ± 0.590	
μ_{IH}	11.97 ± 0.922		10.54 ± 0.860		12.00 ± 0.861		11.68 ± 0.876	
σ_{IH}	29.14 ± 0.652		27.20 ± 0.608		27.24 ± 0.609		27.70 ± 0.619	
$z_{score}^{(NH)}$	1.054	4.040 (app.)	0.963	3.961 (app.)	0.892	3.581 (app.)	0.975	3.747 (app.)
$z_{score}^{(IH)}$	0.971	3.460 (app.)	0.964	3.247 (app.)	0.911	3.464 (app.)	0.944	3.418 (app.)

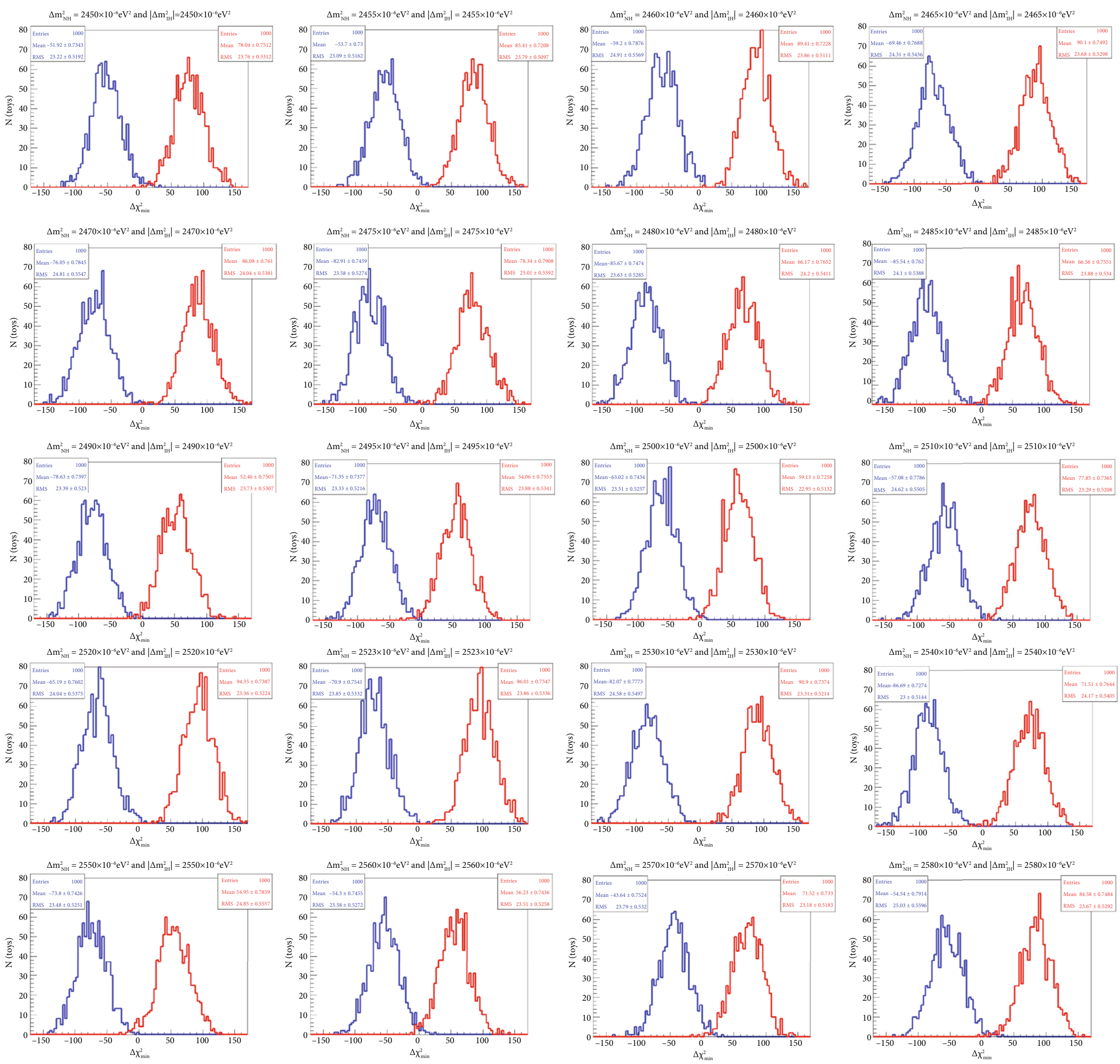

FIGURE 18: $\Delta\chi^2$ estimator for 1000 (NH) + 1000 (IH) toy JUNO-like simulations generated at 20 different values of the atmospheric mass in the range of $2.450 \times 10^{-3}\text{eV}^2 \leq |\Delta m^2| \leq 2.580 \times 10^{-3}\text{eV}^2$ for NH hypothesis (blue distribution in each plot) and IH hypothesis (red distribution in each plot) with six years of exposure and the ten near reactor cores. An infinite energy resolution is assumed. The sensitivities due to these conditions are reported in Table 12.

As mentioned in Section 3, the MH sensitivities using Z-test, $z^{(\text{NH})}_{\text{score}}$ and $z^{(\text{IH})}_{\text{score}}$, do not exactly equal to the MH sensitivities obtained in the approximated Equation (7), $z^{(\text{NH})}_{\text{score}}(\text{app.})$and $z^{(\text{IH})}_{\text{score}}(\text{app.})$. Table 11 reports this observation for 20 different values for the atmospheric mass at infinite energy resolution providing a solid experimental evidence for overestimation behavior for this approximation.

6.2. The Issues of χ^2. Each plot of Figures 19 and 20 proves that χ^2 has not enough ability to produce high sensitivity to distinguish between the right and wrong ordering of the neutrino using the medium baseline reactor spectrum. From the sensitivity tables (Tables 13 and 14), it is clear that the experimental sensitivity using the χ^2 estimator has a strong dependence on the value of the neutrino atmospheric mass. If the neutrino atmospheric mass value is modified, the experimental sensitivity will change according to it, even when the systematic uncertainties are not included.

The results about the standard algorithm confirmed the three statistical issues in the range of $2.450 \times 10^{-3}\text{eV}^2 \leq |\Delta m^2|_{\text{input}} \leq 2.580 \times 10^{-3}\text{eV}^2$.

Table 12: The comparison of the MH sensitivity using $\Delta\chi^2$ assuming infinite energy resolution for NH sample and IH sample, for 20 different values of the atmospheric mass in the range of $2.450 \times 10^{-3} \mathrm{eV}^2 \leq |\Delta m^2| \leq 2.580 \times 10^{-3} \mathrm{eV}^2$. The table indicates the sensitivity calculations using the Z-test for the 1D test in two cases. The first case is without the approximation of Equation (7), and the second one is obtained using the approximation of Equation (7).

Infinite energy resolution								
$\lvert\Delta m^2\rvert_{\mathrm{NH/IH}} \times 10^{-3}$	2.450		2.455		2.460		2.465	
μ_{NH}	−51.90 ± 0.735		−53.72 ± 0.732		−59.20 ± 0.788		−69.43 ± 0.7681	
σ_{NH}	23.24 ± 0.520		23.14 ± 0.518		24.91 ± 0.557		24.29 ± 0.5431	
μ_{IH}	78.03 ± 0.752		85.41 ± 0.720		89.41 ± 0.723		90.09 ± 0.7482	
σ_{IH}	23.77 ± 0.532		22.76 ± 0.520		22.86 ± 0.511		23.65 ± 0.5291	
$z^{(\mathrm{NH})}_{\mathrm{score}}$	5.590	7.204 (app.)	6.013	7.329 (app.)	5.966	7.694 (app.)	6.567	8.332 (app.)
$z^{(\mathrm{IH})}_{\mathrm{score}}$	5.466	8.833 (app.)	6.113	9.242 (app.)	6.501	9.456 (app.)	6.745	9.456 (app.)
$\lvert\Delta m^2\rvert_{\mathrm{NH/IH}} \times 10^{-3}$	2.470		2.475		2.480		2.485	
μ_{NH}	−76.04 ± 0.7834		−82.90 ± 0.7452		−55.70 ± 0.7471		−85.54 ± 0.7595	
σ_{NH}	24.77 ± 0.554		23.55 ± 0.5269		23.62 ± 0.5283		24.29 ± 0.5431	
μ_{IH}	86.13 ± 0.762		78.36 ± 0.7904		66.17 ± 0.7649		90.09 ± 0.7482	
σ_{IH}	24.07 ± 0.5388		24.99 ± 0.5589		24.19 ± 0.5409		23.65 ± 0.5291	
$z^{(\mathrm{NH})}_{\mathrm{score}}$	6.547	8.720 (app.)	6.848	9.105 (app.)	5.160	7.463 (app.)	7.231	9.249 (app.)
$z^{(\mathrm{IH})}_{\mathrm{score}}$	6.737	9.281 (app.)	6.453	8.852 (app.)	5.038	8.134 (app.)	7.426	9.492 (app.)
$\lvert\Delta m^2\rvert_{\mathrm{NH/IH}} \times 10^{-3}$	2.490		2.495		2.500		2.510	
μ_{NH}	−76.63 ± 0.7387		−71.32 ± 0.7365		−63.02 ± 0.743		57.12 ± 0.778	
σ_{NH}	23.36 ± 0.5223		23.29 ± 0.5208		23.51 ± 0.526		24.60 ± 0.550	
μ_{IH}	52.48 ± 0.7507		54.03 ± 0.7557		59.13 ± 0.726		77.89 ± 0.738	
σ_{IH}	23.74 ± 0.5308		23.90 ± 0.5344		22.95 ± 0.513		23.33 ± 0.522	
$z^{(\mathrm{NH})}_{\mathrm{score}}$	5.527	8.445 (app.)	5.382	8.445 (app.)	5.196	7.939 (app.)	5.488	7.556 (app.)
$z^{(\mathrm{IH})}_{\mathrm{score}}$	5.439	7.244 (app.)	5.280	7.351 (app.)	5.322	7.690 (app.)	5.787	8.826 (app.)
$\lvert\Delta m^2\rvert_{\mathrm{NH/IH}} \times 10^{-3}$	2.520		2.523		2.530		2.540	
μ_{NH}	−65.19 ± 0.760		−70.90 ± 0.754		−82.07 ± 0.777		−86.72 ± 0.727	
σ_{NH}	24.04 ± 0.538		23.85 ± 0.533		24.58 ± 0.550		23.00 ± 0.514	
μ_{IH}	94.35 ± 0.739		96.01 ± 0.755		90.90 ± 0.737		71.51 ± 0.762	
σ_{IH}	23.36 ± 0.523		23.89 ± 0.534		23.31 ± 0.521		24.10 ± 0.539	
$z^{(\mathrm{NH})}_{\mathrm{score}}$	6.636	8.074 (app.)	6.998	8.420 (app.)	7.037	9.059 (app.)	6.880	9.312 (app.)
$z^{(\mathrm{IH})}_{\mathrm{score}}$	6.830	9.713 (app.)	6.987	9.798 (app.)	7.420	9.534 (app.)	6.566	8.456 (app.)
$\lvert\Delta m^2\rvert_{\mathrm{NH/IH}} \times 10^{-3}$	2.550		2.560		2.570		2.580	
μ_{NH}	−73.80 ± 0.743		−54.30 ± 0.746		−43.64 ± 0.752		−54.54 ± 0.791	
σ_{NH}	23.48 ± 0.525		23.58 ± 0.527		23.79 ± 0.532		25.03 ± 0.560	
μ_{IH}	54.95 ± 0.786		56.23 ± 0.744		71.52 ± 0.733		84.58 ± 0.748	
σ_{IH}	24.85 ± 0.556		23.51 ± 0.526		23.18 ± 0.518		23.67 ± 0.529	
$z^{(\mathrm{NH})}_{\mathrm{score}}$	5.483	8.591 (app.)	4.687	7.369 (app.)	4.841	6.606 (app.)	5.848	7.385 (app.)
$z^{(\mathrm{IH})}_{\mathrm{score}}$	5.181	7.413 (app.)	4.701	7.50 (app.)	5.0	8.457 (app.)	5.877	9.197 (app.)

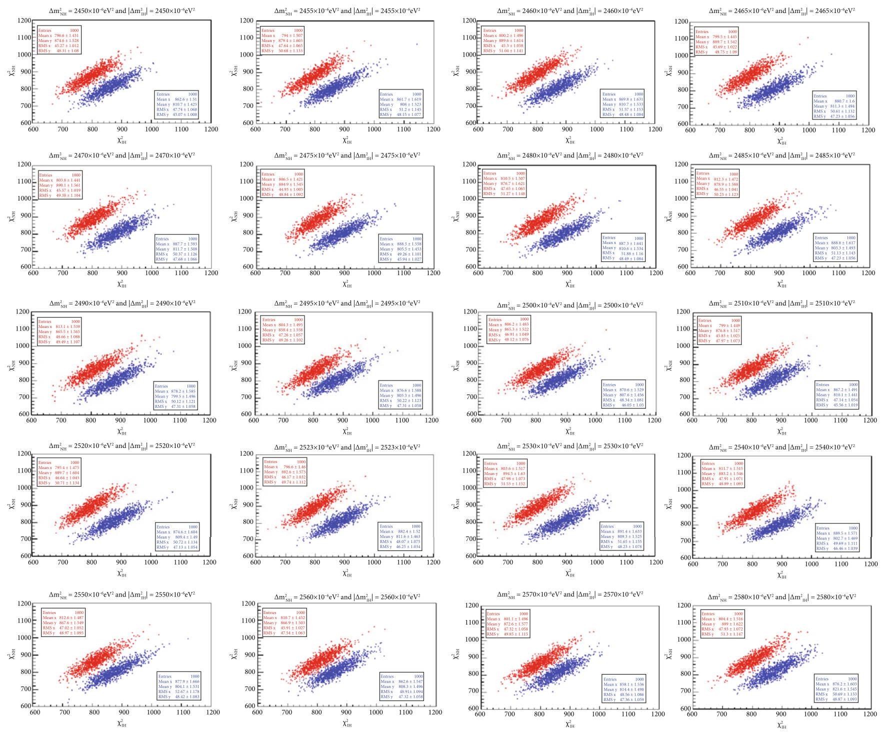

Figure 19: Two χ^2 distributions for 1000 (NH) + 1000 (IH) toy JUNO-like simulations that generated at 20 different values of the atmospheric mass in the range of $2.450 \times 10^{-3} \mathrm{eV}^2 \leq |\Delta m^2| \leq 2.580 \times 10^{-3} \mathrm{eV}^2$ for NH hypothesis (blue distribution in each plot) and IH hypothesis (blue distribution in each plot) with six years of exposure and the ten near reactor cores with infinite energy resolution. The sensitivities due to these conditions are reported in Table 13.

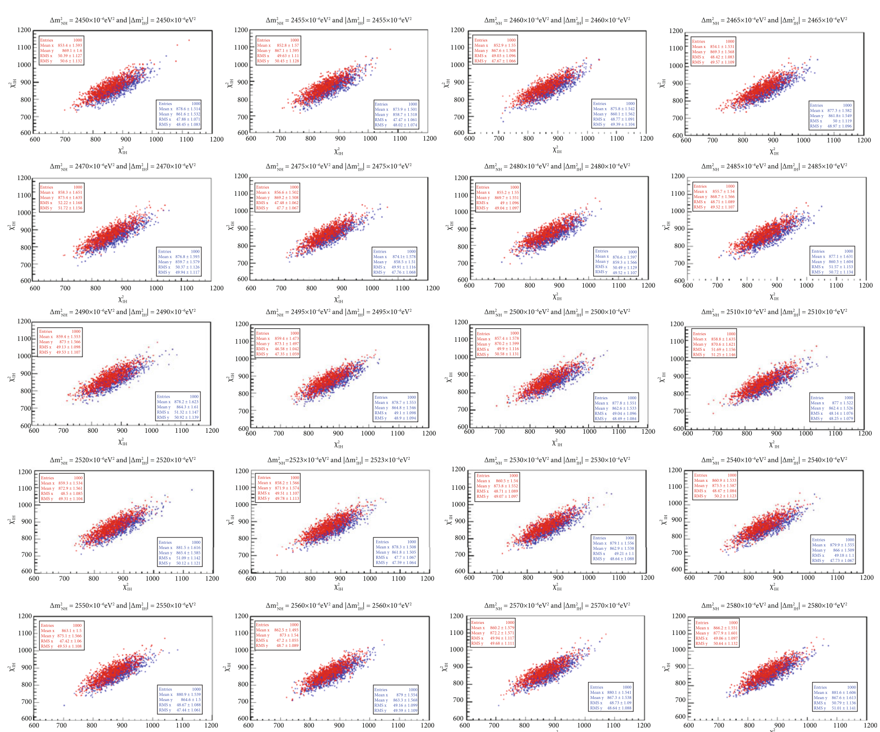

Figure 20: Two $\chi 2$ distributions for 1000 (NH) + 1000 (IH) toy JUNO-like simulations generated at 20 different values of the atmospheric mass in the range of $2.450 \times 10^{-3} \mathrm{eV}^2 \leq |\Delta m^2|_{\mathrm{input}} \leq 2.580 \times 10^{-3} \mathrm{eV}^2$ for NH hypothesis (blue distribution in each plot) and IH hypothesis (blue distribution in each plot) with six years of exposure and the ten near reactor cores, with energy resolution $3\%/\sqrt{E}$. The sensitivities due to these conditions are reported in Table 14.

Table 13: The comparison of the MH sensitivity using χ^2 as a bidimensional estimator assuming infinite energy resolution for NH sample and IH sample, for 20 different values of the atmospheric mass in the range of $2.450 \times 10^{-3}\,\text{eV}^2 \leq |\Delta m^2| \leq 2.580 \times 10^{-3}\,\text{eV}^2$. The table indicates the sensitivity calculations using the Z-test for 2D.

Infinite energy resolution										
$\lvert\Delta m^2\rvert_{NH/IH} \times 10^{-3}$	2.450		2.455		2.460		2.465		2.470	
	NH	IH	NH	IH	NH	IH	NH	IH	NH	IH
μ_{NH}	810.7 ± 1.425	874.6 ± 1.528	808 ± 1.523	879.4 ± 1.602	810.7 ± 1.533	889.6 ± 1.614	811.3 ± 1.494	889.7 ± 1.542	811.7 ± 1.593	890.1 ± 1.441
σ_{NH}	45.07 ± 1.008	48.31 ± 1.080	48.17 ± 1.077	50.67 ± 1.133	48.48 ± 1.084	51.04 ± 1.141	47.23 ± 1.056	48.76 ± 1.090	47.7 ± 1.067	49.39 ± 1.104
μ_{IH}	862.6 ± 1.510	796.6 ± 1.432	861.7 ± 1.619	794 ± 1.507	869.8 ± 1.631	800.2 ± 1.496	880.7 ± 1.601	799.5 ± 1.445	887.7 ± 1.593	803.8 ± 1.441
σ_{IH}	47.75 ± 1.068	45.27 ± 1.012	51.2 ± 1.145	47.67 ± 1.066	51.57 ± 1.153	47.3 ± 1.058	50.62 ± 1.132	45.69 ± 1.022	50.39 ± 1.127	45.57 ± 1.019
$z_{score}^{(NH)}$	1.0095		1.0154		1.0717		1.163		1.1728	
$z_{score}^{(IH)}$	1.0013		1.0261		1.0891		1.2050		1.2113	
$\lvert\Delta m^2\rvert_{NH/IH} \times 10^{-3}$	2.475		2.480		2.485		2.490		2.495	
	NH	IH	NH	IH	NH	IH	NH	IH	NH	IH
μ_{NH}	811.7 ± 1.508	890.1 ± 1.562	805.5 ± 1.453	884.9 ± 1.545	801.3 ± 1.641	876.7 ± 1.622	799.6 ± 1.496	865.5 ± 1.565	805.3 ± 1.495	858.4 ± 1.558
σ_{NH}	47.7 ± 1.067	49.39 ± 1.104	45.94 ± 1.027	48.85 ± 1.092	48.48 ± 1.084	51.28 ± 1.147	47.32 ± 1.058	49.50 ± 1.107	47.28 ± 1.057	49.28 ± 1.102
μ_{IH}	887.7 ± 1.593	803.8 ± 1.441	888.5 ± 1.558	806.5 ± 1.420	887.3 ± 1.641	810.5 ± 1.507	878.2 ± 1.585	813.10 ± 1.539	876.6 ± 1.588	804.3 ± 1.495
σ_{IH}	50.39 ± 1.127	45.57 ± 1.019	49.26 ± 1.102	44.92	51.9 ± 1.084	47.64 ± 1.065	50.11 ± 1.121	48.66 ± 1.088	47.28 ± 1.057	47.27 ± 1.057
$z_{score}^{(NH)}$	1.1990		1.0786		1.102		0.9703		0.9177	
$z_{score}^{(IH)}$	1.2172		1.0944		1.1201		0.9632		0.9268	
$\lvert\Delta m^2\rvert_{NH/IH} \times 10^{-3}$	2.500		2.510		2.520		2.523		2.530	
	NH	IH	NH	IH	NH	IH	NH	IH	NH	IH
μ_{NH}	807.6 ± 1.456	865.3 ± 1.522	810.10 ± 1.491	876.90 ± 1.516	809.4 ± 1.49	889.7 ± 1.604	811.6 ± 1.463	892.6 ± 1.573	809.3 ± 1.525	894.5 ± 1.630
σ_{NH}	46.05 ± 1.03	48.12 ± 1.076	45.57 ± 1.019	47.95 ± 1.072	47.13 ± 1.054	50.71 ± 1.134	46.25 ± 1.034	49.74 ± 1.112	48.23 ± 1.078	51.53 ± 1.152
μ_{IH}	870.6 ± 1.529	806.2 ± 1.483	867.2 ± 1.491	799 ± 1.449	874.6 ± 1.604	795.4 ± 1.475	882.4 ± 1.52	796.6 ± 1.460	891.4 ± 1.633	803.6 ± 1.517
σ_{IH}	48.34 ± 1.081	46.91 ± 1.049	47.14 ± 1.054	45.83 ± 1.516	50.72 ± 1.134	46.64 ± 1.043	48.07 ± 1.075	46.17 ± 1.032	51.65 ± 1.155	51.53 ± 1.152
$z_{score}^{(NH)}$	0.9159		1.0418		1.1720		1.2647		1.226	
$z_{score}^{(IH)}$	0.9099		1.0200		1.1781		1.2442		1.231	

TABLE 13: Continued.

Infinite energy resolution										
$\lvert\Delta m^2\rvert_{NH/IH} \times 10^{-3}$	2.540		2.550		2.560		2.570		2.580	
	NH	IH	NH	IH	NH	IH	NH	IH	NH	IH
μ_{NH}	802.7 ± 1.469	883.2 ± 1.546	804.1 ± 1.531	867.6 ± 1.549	862.6 ± 1.547	866.9 ± 1.503	814.4 ± 1.498	872.6 ± 1.577	821.6 ± 1.545	889 ± 1.622
σ_{NH}	46.47 ± 1.039	48.89 ± 1.093	48.42 ± 1.083	48.97 ± 1.095	47.32 ± 1.058	47.54 ± 1.063	47.36 ± 1.059	49.85 ± 1.115	48.87 ± 1.093	51.3 ± 1.147
μ_{IH}	889.5 ± 1.571	811.7 ± 1.515	877.90 ± 1.666	812.6 ± 1.487	808.3 ± 1.496	810.7 ± 1.452	858.1 ± 1.536	801.1 ± 1.496	876.2 ± 1.603	804.4 ± 1.516
σ_{IH}	49.68 ± 1.111	47.91 ± 1.071	48.42 ± 1.083	47.02 ± 1.052	48.91 ± 1.058	45.91 ± 1.027	48.56 ± 1.086	47.32 ± 1.058	50.69 ± 1.133	47.93 ± 1.072
$z_{score}^{(NH)}$	1.1690		0.9103		0.8122		0.8734		1.0111	
$z_{score}^{(IH)}$	1.1613		0.9586		0.8364		0.8622		1.0144	

Table 14: The comparison of the MH sensitivity using χ^2 as a bidimensional estimator for actual distributions for NH sample and IH sample, for 20 different values of the atmospheric mass in the range of $2.450 \times 10^{-3} \mathrm{eV}^2 \leq |\Delta m^2|_{\mathrm{input}} \leq 2.580 \times 10^{-3} \mathrm{eV}^2$. The table indicates the sensitivity calculations using the Z-test for the 2D test.

Relative energy resolution $3\%/\sqrt{E}$										
$\|\Delta m^2\|_{\mathrm{NH/IH}} \times 10^{-3}$	2.450		2.455		2.460		2.465		2.470	
	NH	IH	NH	IH	NH	IH	NH	IH	NH	IH
μ_{NH}	861.7 ± 1.532	869.1 ± 1.601	858.7 ± 1.519	867.1 ± 1.596	860.1 ± 1.542	867.6 ± 1.508	861.8 ± 1.549	869.4 ± 1.567	864.4 ± 1.61	873 ± 1.566
σ_{NH}	48.45 ± 1.083	50.61 ± 1.127	48.03 ± 1.074	50.46 ± 1.128	49.39 ± 1.104	47.67 ± 1.066	48.97 ± 1.096	49.57 ± 1.108	50.90 ± 1.138	49.54 ± 1.108
μ_{IH}	878.6 ± 1.514	853.4 ± 1.594	873.8 ± 1.501	852.8 ± 1.570	875.8 ± 1.542	852.9 ± 1.55	877.3 ± 1.582	854.1 ± 1.531	878.2 ± 1.623	859.4 ± 1.554
σ_{IH}	48.45 ± 1.083	50.41 ± 1.132	47.48 ± 1.062	49.64 ± 1.110	48.77 ± 1.091	49.03 ± 1.096	50 ± 1.119	49.57 ± 1.108	51.31 ± 1.147	49.14 ± 1.099
$z_{\mathrm{score}}^{(\mathrm{NH})}$	0.2397		0.2184		0.2194		0.2198		0.2273	
$z_{\mathrm{score}}^{(\mathrm{IH})}$	0.2286		0.2084		0.2227		0.2220		0.2193	
$\|\Delta m^2\|_{\mathrm{NH/IH}} \times 10^{-3}$	2.475		2.480		2.485		2.490		2.495	
	NH	IH	NH	IH	NH	IH	NH	IH	NH	IH
μ_{NH}	858.5 ± 1.511	869.2 ± 1.509	859.4 ± 1.566	869.7 ± 1.551	860.3 ± 1.604	868.7 ± 1.565	864.4 ± 1.61	873 ± 1.566	864.8 ± 1.546	873 ± 1.497
σ_{NH}	47.77 ± 1.068	47.73 ± 1.067	49.51 ± 1.107	49.05 ± 1.097	50.71 ± 1.134	49.50 ± 1.107	50.9 ± 1.138	49.54 ± 1.108	48.89 ± 1.093	47.35 ± 1.059
μ_{IH}	874.1 ± 1.578	856.7 ± 1.502	876.6 ± 1.596	855.2 ± 1.55	877.1 ± 1.631	855.7 ± 1.54	878.2 ± 1.623	859.4 ± 1554	878.7 ± 1.553	859.4 ± 1.473
σ_{IH}	49.89 ± 1.116	47.49 ± 1.062	50.46 ± 1.128	49.05 ± 1.097	51.57 ± 1.153	48.71 ± 1.089	51.31 ± 1.147	49.14 ± 1.099	49.10 ± 1.098	46.6 ± 1.059
$z_{\mathrm{score}}^{(\mathrm{NH})}$	0.2045		0.2250		0.2073		0.1898		0.1983	
$z_{\mathrm{score}}^{(\mathrm{IH})}$	0.2098		0.2294		0.2159		0.1967		0.2068	
$\|\Delta m^2\|_{\mathrm{NH/IH}} \times 10^{-3}$	2.500		2.510		2.520		2.523		2.530	
	NH	IH	NH	IH	NH	IH	NH	IH	NH	IH
μ_{NH}	862.6 ± 1.533	870.2 ± 1.599	862.4 ± 1.526	870.6 ± 1.621	865.4 ± 1.585	872.9 ± 1.561	861.8 ± 1.505	871.9 ± 1.574	862.9 ± 1.538	873.8 ± 1.552
σ_{NH}	48.49 ± 1.084	50.58 ± 1.131	48.24 ± 1.079	51.68 ± 1.156	50.12 ± 1.121	49.37 ± 1.104	47.59 ± 1.064	49.78 ± 1.113	48.64 ± 1.088	49.07 ± 1.097
μ_{IH}	877.8 ± 1.551	857.4 ± 1.578	877 ± 152	858.8 ± 1.634	881.5 ± 1.616	859.3 ± 1.534	878.3 ± 1.508	858.2 ± 1.566	879.1 ± 1.556	860.5 ± 1.54
σ_{IH}	49.04 ± 1.096	49.90 ± 1.116	48.14 ± 1.08	51.25 ± 1.146	51.09 ± 1.142	48.50 ± 1.065	47.7 ± 1.067	49.51 ± 1.107	49.21 ± 1.10	860.5 ± 1.54
$z_{\mathrm{score}}^{(\mathrm{NH})}$	0.2040		0.1945		0.2083		0.2253		0.2145	
$z_{\mathrm{score}}^{(\mathrm{IH})}$	0.1980		0.1822		0.2153		0.2164		0.2146	

Table 14: Continued.

Relative energy resolution $3\%/\sqrt{E}$										
$\left|\Delta m^2\right|_{NH/IH} \times 10^{-3}$	2.540		2.550		2.560		2.570		2.580	
	NH	IH	NH	IH	NH	IH	NH	IH	NH	IH
μ_{NH}	866.0 ± 1.509	873.5 ± 1.587	864.6 ± 1.50	875.1 ± 1.566	863.3 ± 1.568	873.0 ± 1.540	867.3 ± 1.538	872.2 ± 1.571	867.6 ± 1.613	877.9 ± 1.601
σ_{NH}	47.73 ± 1.067	50.19 ± 1.122	47.44 ± 1.061	49.53 ± 1.108	49.59 ± 1.109	48.70 ± 1.089	48.64 ± 1.088	49.68 ± 1.111	51.01 ± 1.141	50.64 ± 1.132
μ_{IH}	879.9 ± 1.555	860.9 ± 1.533	880.9 ± 1539	863.1 ± 1.5	879.0 ± 1.554	862.5 ± 1.493	880.1 ± 1.541	860.2 ± 1.579	881.6 ± 1.606	866.20 ± 1.551
σ_{IH}	49.17 ± 1.067	48.47 ± 1.084	48.67 ± 1.061	47.42 ± 1.06	49.16 ± 1.099	47.2 ± 1.055	48.73 ± 1.09	49.941.117	50.79 ± 1.136	49.06 ± 1.097
$z_{score}^{(NH)}$	0.1936		0.2104		0.1909		0.1803		0.1793	
$z_{score}^{(IH)}$	0.1902		0.2086		0.1966		0.1763		0.1831	

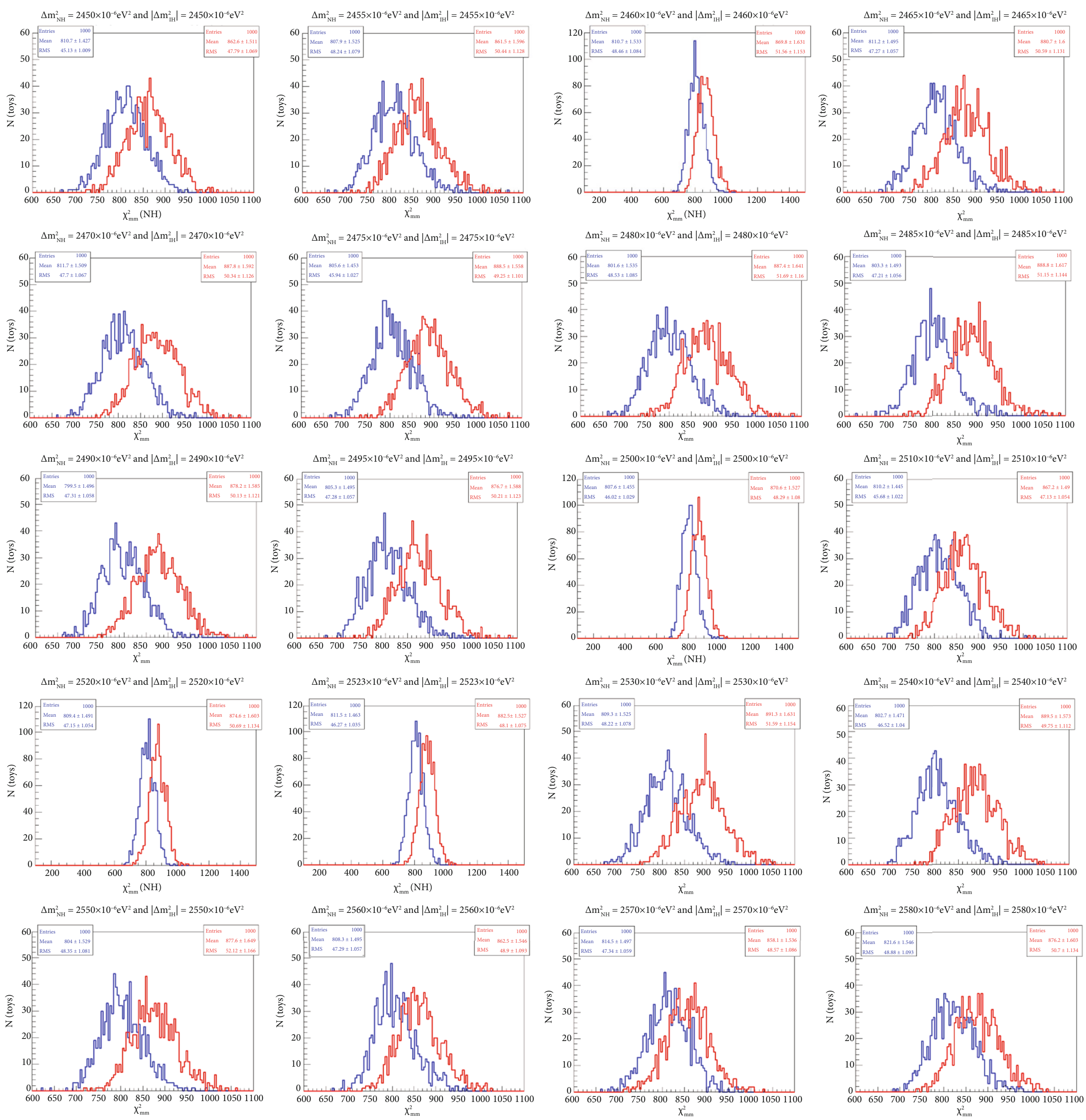

FIGURE 21: χ^2 distributions for 1000 toy JUNO-like simulations generated for NH samples at 20 different values of the atmospheric mass in the range of $2.450\times10^{-3}\text{eV}^2 \le |\Delta m^2|_{\text{input}} \le 2.580\times10^{-3}\text{eV}^2$ for NH hypothesis (blue graphs) and for IH hypothesis (red graphs) with six years of exposure and the ten near reactor cores with an infinite energy resolution.

7. Conclusion

Advances in statistical methods may play a decisive role in the discovery reachable at neutrino physics experiments. Evaluating the used statistical methods and updating them is a necessary step in building a robust statistical analysis for answering the open questions in neutrino physics [20]. The statistical issues on the ν MHD from the reactor experiments have been illustrated, starting from the limited power of the $\Delta\chi^2$. When the simulation is performed on an event–by–event basis and not on a semianalytical one, the significance drastically drops. In fact, the systematic uncertainties due to the 3% relatively energy resolution cause unbalanced migration effects between events that do not show up when the simulations are not made on an event–by–event basis. To confirm the effect, simulations at infinite energy resolution have also been performed confirming the validation of the assumption of Equation (7) in case of exclusion of the systematic uncertainties. $\Delta\chi^2$ is fully controlled by the statistical assumptions as explained in

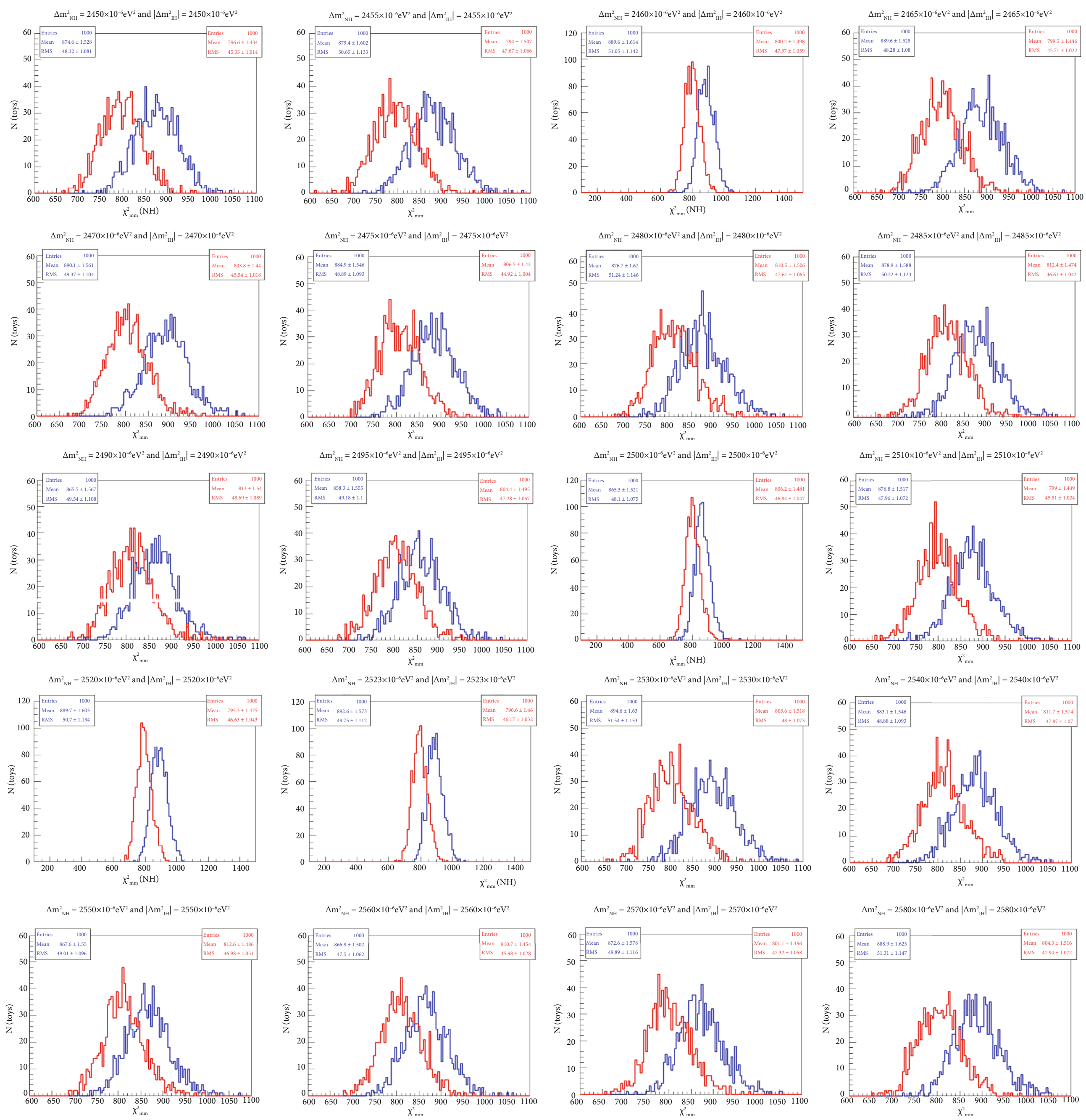

Figure 22: χ^2 distributions for 1000 toy JUNO-like simulations generated for IH samples at 20 different values of the atmospheric mass in the range of $2.450 \times 10^{-3}\text{eV}^2 \leq |\Delta m^2|_{\text{input}} \leq 2.580 \times 10^{-3}\text{eV}^2$ for NH hypothesis (blue graphs) and for IH hypothesis (red graphs) with six years of exposure and the ten near reactor cores with an infinite energy resolution.

Section 3. That is the major limit to the approximation, reducing the experimental standard sensitivity that is officially reported. To conclude this first issue, it has been pointed out that the $\Delta\chi^2$ estimator provides us with different results following different simulation procedures. Second, the strong positive correlations between the $\chi^2_{\text{min (NH)}}$ and $\chi^2_{\text{min (IH)}}$ when they are drawn in a 2-dimensional map confirms the $\chi^2 = (\chi^2_{\text{min (IH)}}, \chi^2_{\text{min (NH)}})$ being a bidimensional estimator. As a second issue, we then conclude that JUNO sensitivity using χ^2 as bidimensional estimator is not promising as well. Third, the $\Delta\chi^2$ is dominated by the $|\Delta m^2|_{\text{input}}$ value as described in dx_dm. Then, the MHD significance using $|\overline{\Delta\chi^2}|$ depends on the values of the input parameter $|\Delta m^2|_{\text{input}}$. That is the reason we were interested in studying the MHD problem by using the standard method at 20 different values of $|\Delta m^2|_{\text{input}}$ in the range between $2.450 \times 10^{-3}\text{eV}^2$ and $2.580 \times 10^{-3}\text{eV}^2$.

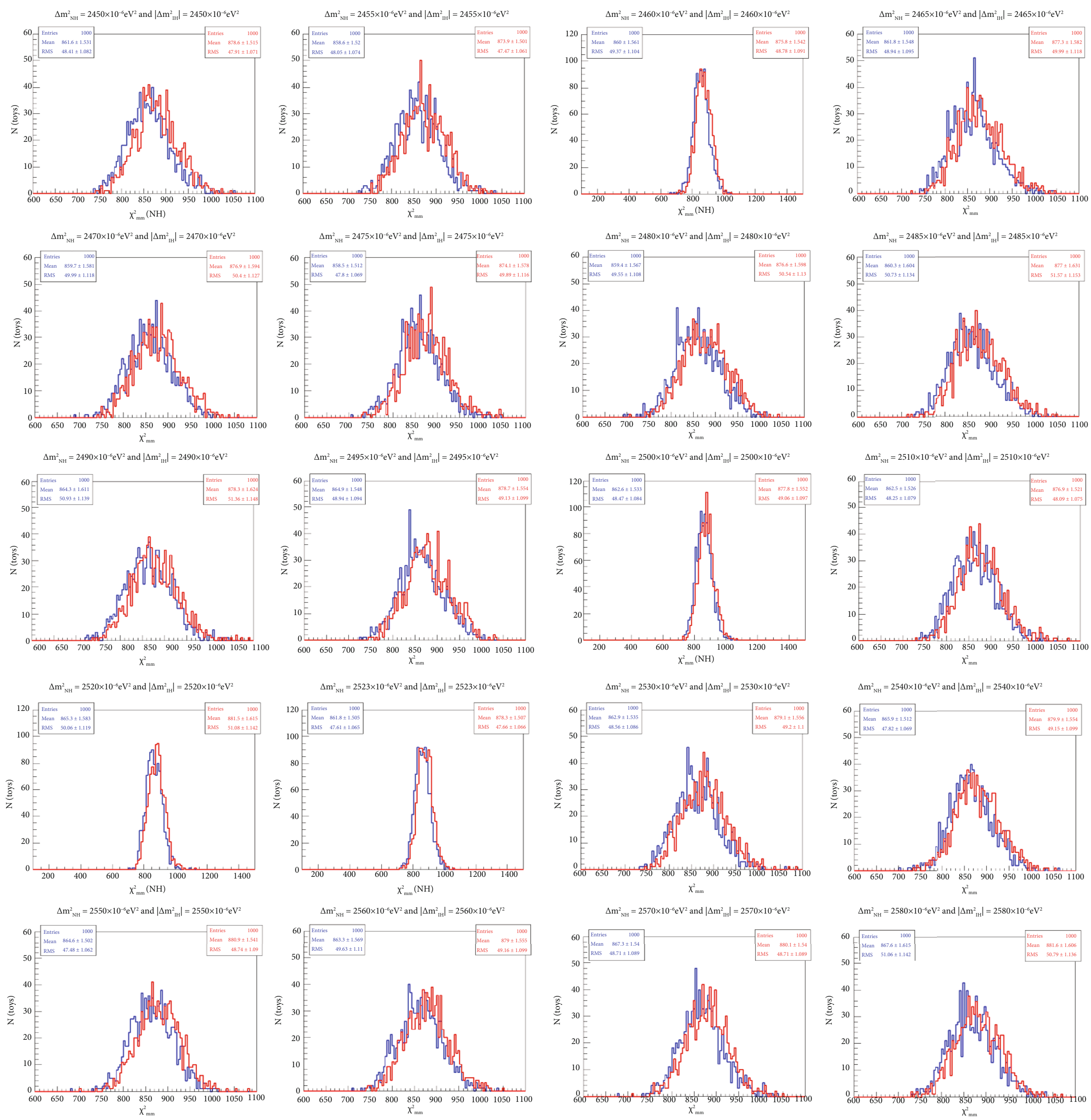

Figure 23: χ^2 distributions for 1000 toy JUNO-like simulations generated for NH samples at 20 different values of the atmospheric mass in the range of $2.450 \times 10^{-3} \mathrm{eV}^2 \leq |\Delta m^2|_{\mathrm{input}} \leq 2.580 \times 10^{-3} \mathrm{eV}^2$ for NH hypothesis (blue graphs) and for IH hypothesis (red graphs) with six years of exposure and the ten near reactor cores with an $3\%/\sqrt{E}$ energy resolution.

Appendix

Fitting with TMinuit Class

Toy simulations were based on a single event basis and the expected systematic errors via a Gaussian distribution centered at the expected mean and with the standard deviation of the estimated uncertainty can be added. For JUNO, a global $3\%/\sqrt{E}(\mathrm{MeV})$ resolution on the energy reconstruction is expected. The oscillation parameters have been taken from the most recent global fits listed in Table 1. The Poisson statistical fluctuation is automatically included.

The fitting procedures and the minimization of χ^2 are done via the ROOT minimization libraries (the TMinuit algorithm). In the minimization procedure, all the oscillation parameters were fixed to the best-fitting values of [8]. A total of 108357 signal events are processed for each toy simulations. The official version of JUNO Software "J17v1r1" is used. $\Delta\chi^2$ will be often scaled with the number

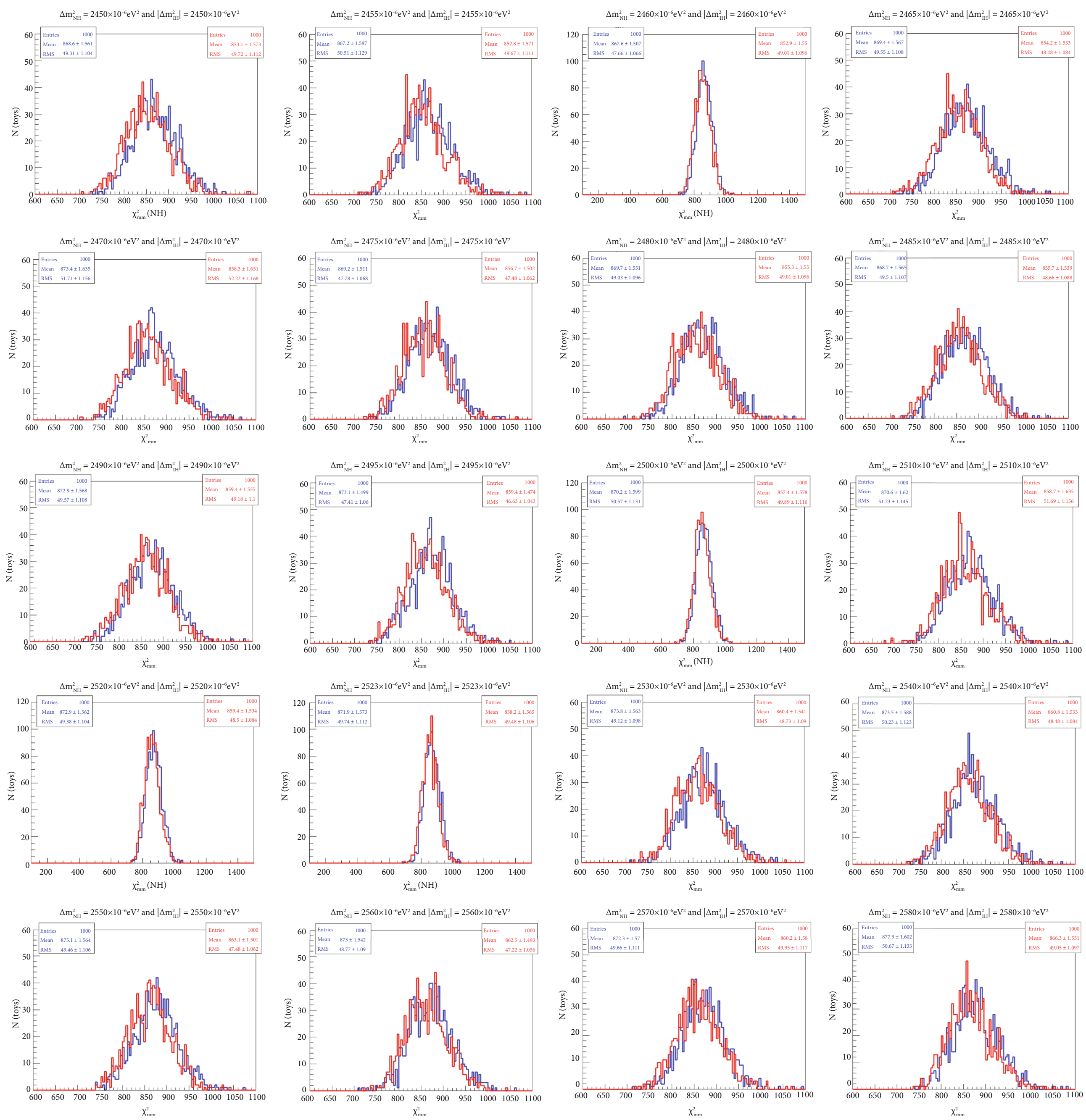

Figure 24: χ^2 distributions for 1000 toy JUNO-like simulations generated for IH samples at 20 different values of the atmospheric mass in the range of $2.450 \times 10^{-3}\mathrm{eV}^2 \leq |\Delta m^2|_{input} \leq 2.580 \times 10^{-3}\mathrm{eV}^2$ for NH hypothesis (blue graphs) and for IH hypothesis (red graphs) with six years of exposure and the ten near reactor cores with an $3\%/\sqrt{E}$ energy resolution.

of degrees of freedom, which is clearly equal to the number of fitted data minus the constraints: *bin*–6. Figures 21 and 22 indicate χ^2 distributions for 1000 toy JUNO-like simulations generated for NH and IH samples, respectively. The simulations are generated at 20 different values of the atmospheric mass in the range of $2.450 \times 10^{-3}\mathrm{eV}^2 \leq |\Delta m^2|_{\mathrm{input}} \leq 2.580 \times 10^{-3}\mathrm{eV}^2$ for NH hypothesis (blue graphs) and for IH hypothesis (red graphs) with six years of exposure and the ten near reactor cores with an infinite energy resolution. Figures 23 and 24 indicate the χ^2 distributions for 1000 toy JUNO-like simulations generated for NH and IH samples, respectively. The simulations are generated at 20 different values of the atmospheric mass in the range of $2.450 \times 10^{-3}\mathrm{eV}^2 \leq |\Delta m^2|_{\mathrm{input}} \leq 2.580 \times 10^{-3}\mathrm{eV}^2$ for NH hypothesis (blue graphs) and for IH hypothesis (red graphs) with six years of exposure and the ten near reactor cores with an $3\%/\sqrt{E}$ energy resolution.

Data Availability

The statistical sample data used to support the findings of this study are included within the article.

Disclosure

An arXiv has previously been published [21]. The arXiv version of the paper is at https://arxiv.org/abs/2310.01814.

Conflicts of Interest

The authors declare that they have no conflicts of interest.

Acknowledgments

We are particularly grateful to Xuefeng Ding for valuable suggestions on the robustness of $\Delta\chi^2$. The article is written with the financial contribution from Fondazione Cariparo in the Dipartimento di Fisica e Astronomia "Galileo Galilei," University of Padova, Italy, and INFN, Padova station, Italy.

References

[1] L. Stanco, "A view of neutrino studies with the next generation facilities," *Reviews in Physics*, vol. 1, pp. 90–100, 2016.

[2] F. Iachello, "Open problems in neutrino physics," *Journal of Physics: Conference Series*, vol. 1056, article 012027, 2018.

[3] W. Rodejohann, "Neutrino-less double beta decay and particle physics," *International Journal of Modern Physics E*, vol. 20, no. 9, pp. 1833–1930, 2011.

[4] Z. Xing and S. Zhou, *Neutrinos in Particle Physics, Astronomy and Cosmology*, Springer Science & Business Media, 2011.

[5] W. H. Furry, "On transition probabilities in double beta disintegration," *Physical Review*, vol. 56, no. 12, p. 1184, 1939.

[6] S. T. Petcov, "The nature of massive neutrinos," *Advances in High Energy Physics*, vol. 2013, Article ID 852987, 20 pages, 2013.

[7] S. M. Bilenky, F. Capozzi, and S. T. Petcov, "An alternative method of determining the neutrino mass ordering in reactor neutrino experiments," *Physics Letters B*, vol. 772, pp. 179–183, 2017.

[8] A. Fengpeng, A. Guangpeng, E. Baussan et al., "Neutrino physics with JUNO," *Journal of Physics G: Nuclear and Particle Physics*, vol. 43, no. 3, article 030401, 2016.

[9] C. Sandhya, S. T. Petcov, and M. Piai, "Precision neutrino oscillation physics with an intermediate baseline reactor neutrino experiment," *Physical Review D*, vol. 68, no. 11, article 113006, 2003.

[10] L. Stanco, G. Salamanna, A. Lokhov, F. Sawy, and C. Sirignano, "A new way to determine the neutrino mass hierarchy at reactors," 2017, https://arxiv.org/1707.07651.

[11] Y.-F. Li, J. Cao, Y. Wang, and L. Zhan, "Unambiguous determination of the neutrino mass hierarchy using reactor neutrinos," *Physical Review D*, vol. 88, no. 1, article 013008, 2013.

[12] F. Capozzi, E. Di Valentino, E. Lisi, A. Marrone, A. Melchiorri, and A. Palazzo, "Global constraints on absolute neutrino masses and their ordering," *Physical Review D*, vol. 95, no. 9, article 096014, 2017.

[13] S.-F. Ge, K. Hagiwara, N. Okamura, and Y. Takaesu, "Determination of mass hierarchy with medium baseline reactor neutrino experiments," *Journal of High Energy Physics*, vol. 2013, no. 5, p. 131, 2013.

[14] E. Ciuffoli, J. Evslin, and X. Zhang, "Confidence in a neutrino mass hierarchy determination," *Journal of High Energy Physics*, vol. 2014, no. 1, p. 95, 2014.

[15] "Valencia-Globalfit," http://globalfit.astroparticles.es/ 2018.

[16] P. F. de Salas, S. Gariazzo, O. Mena, C. A. Ternes, and M. Tórtola, "Neutrino mass ordering from oscillations and beyond: 2018 status and future prospects," *Frontiers in Astronomy and Space Sciences*, vol. 5, 2018.

[17] S. Gariazzo, M. Archidiacono, P. F. de Salas, O. Mena, C. A. Ternes, and M. Tórtola, "Neutrino masses and their ordering: global data, priors and models," *Journal of Cosmology and Astroparticle Physics*, vol. 2018, no. 3, 2018.

[18] P. Linsley, P. Shrives, and M. Wieczorek-Kosmala, "Multiple perspectives in risk and risk management: ERRN 8th European Risk Conference 2018, Katowice, Poland, September 20 – 21," in *Springer Proceedings in Business and Economics*, Springer International Publishing, 2019, https://books.google.com.eg/books?id=ZsiSDwAAQBAJ.

[19] P. J. Huber, "Robust statistics," in *Wiley Series in Probability and Mathematical Statistics*, John Wiley & Sons, Inc., New York, 1981.

[20] https://agenda.infn.it/event/18760/contributions/87947/attachments/62821/75485/FatmaFerraraMay20194.

[21] F. Sawy and L. Stanco, "Statistical issues on the neutrino mass hierarchy with $\Delta\chi^2$," 2023, https://arxiv.org/abs/2310.01814.